J. Fluid Mech. (1994), *vol.* 274, *pp.* 349–381

Shock waves in dilute bubbly liquids

By M. WATANABE AND A. PROSPERETTI
Department of Mechanical Engineering, The Johns Hopkins University, Baltimore, MD 21218, USA

(Received 11 June 1992 and in revised form 28 March 1994)

The propagation of weak shock waves in liquids containing a small concentration of gas bubbles is studied theoretically on the basis of a mathematical model that contains all – and only – the effects that contribute to first order in the gas volume fraction. In particular, the thermal exchange between the gas bubbles and the liquid is described accurately. This aspect of the theory emerges as its most significant component, relegating effects such as the relative motion between the phases to roles of minor importance. Comparison with experimental results substantiates the accuracy of the model for shock waves that have had time to broaden from an initial sharp front to a more diffuse profile. For shock waves closer to inception, marked differences are found between theory and experiment. The same problem affects all other published theoretical treatments. It is concluded that some as yet poorly understood mechanism governs the early-time behaviour of shock waves in bubbly liquids.

1. Introduction

Among multi-phase systems, liquids containing gas bubbles have some unique features that render them particularly interesting. In the first place, even a minute bubble concentration greatly increases the compressibility of the medium and has therefore a drastic effect on its properties. Secondly, compared with suspensions, emulsions, or fluidized beds, the inhomogeneities of bubbly liquids – the bubbles – have a particularly rich internal structure that endows the medium with a strikingly complex behaviour even at dilute concentrations. The latter feature justifies the approach taken in this paper which constitutes in a certain sense a reversal of the one common in multi-phase flows in which the focus is on the average behaviour of the system rather than on the micromechanics of the disperse phase.

Here we are not so much interested in 'improving' two-phase flow models by incorporating, on the basis of physical intuition, specific features such as inter-phase drag or mutual interactions among the bubbles. Rather, our intent is to investigate how far a model mathematically correct to first order in the gas volume fraction can go in explaining the observed behaviour of bubbly liquids. While the formulation of an (or *the*) 'ultimate' model must of course remain the final objective of theoretical research in multi-phase flow, it is useful to establish a baseline for the strengths and limitations of the presently available rigorous models. As a consequence of this premise, our model for the gas–liquid mixture, although correct in the dilute limit we consider, is comparatively simple, while the bubbles are described in detail. This approach is justified by the fact that the internal thermo-fluid mechanics of the gas is essentially independent of the bubble concentration so that a model of bubbly liquids should incorporate the effects that are known to be important even at zero gas volume fractions, i.e. in the case of single bubbles.

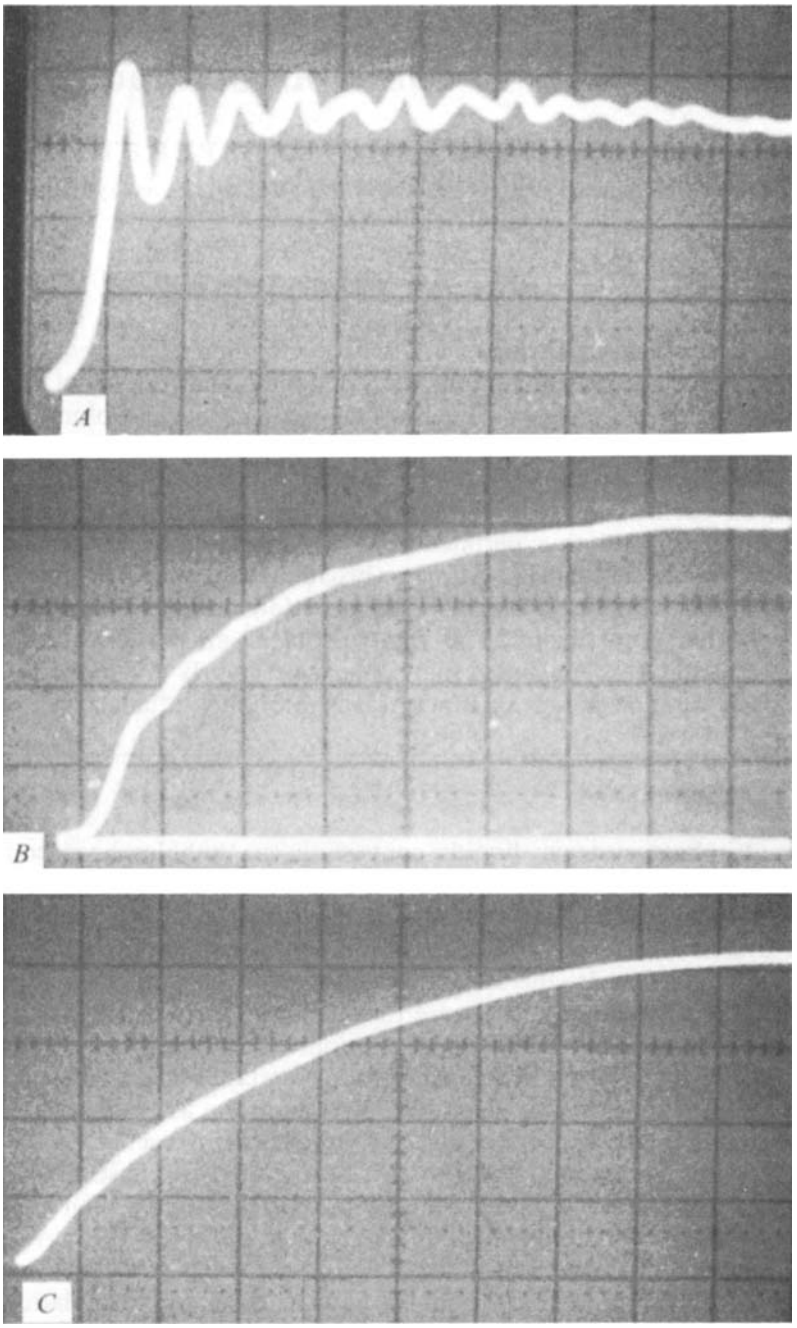

FIGURE 1. Typical waveforms observed during the propagation of shocks in bubbly liquids (reproduced with permission from Noordzij & van Wijngaarden 1974). The three types are referred to as *A*-, *B*-, and *C*-type waves.

Figure 1 (from Noordzij & van Wijngaarden 1974) shows the three typical pressure waveforms observed in a 'shock-tube' experiment with a bubbly liquid. The top, highly oscillatory one (type *A*) is usually found near the boundary at which the shock is introduced. The other two (types *B* and *C*) represent later stages in the evolution of the

wave. Our results indicate that the inclusion of a detailed modelling of the gas thermal behaviour is sufficient to give a satisfactory agreement with the data for the *B*- and *C*-type shocks taken by Noordzij (1973) in mixtures with a maximum gas volume fraction of the order of 3%. Significant discrepancies, however, are found in the case of *A* shocks.

To study the origin of these discrepancies, in §6 we consider the magnitude of some of the effects that would typically be included in more developed models. As with several previous investigations, the conclusion is that, while data can be matched by suitably adjusting parameters, the values required are outside the expected range and, in some cases, even have the opposite sign. As none of the physical processes studied so far by ourselves or others seems able to account for the differences with experiment, their origin appears to be due to as yet unexplained mechanisms.

Much of the previous work on shock waves in bubbly liquids is referenced and discussed in §§6 and 7. It is however appropriate to mention here the seminal studies of Noordzij & van Wijngaarden (1974) and Nigmatulin & Shagapov (1974). Nigmatulin and co-workers have published a large number of papers on this problem which have recently been summarized in Nigmatulin (1991). In particular, Nigmatulin was the first to recognize the importance of thermal effects on the shock dynamics. Beylich & Gülhan (1990) have also published new data on *A*-type shocks and made an effort to incorporate in their model many physical effects.

2. Mathematical model

Caflisch *et al.* (1985) obtained the following mathematical formulation for the description of pressure waves in a bubbly liquid:

$$\frac{1}{\rho_L c_L^2}\frac{\partial P}{\partial t}+\nabla\cdot\boldsymbol{u}=4\pi nR^2\frac{\partial R}{\partial t}, \tag{1}$$

$$\rho_L\frac{\partial \boldsymbol{u}}{\partial t}+\nabla P=0. \tag{2}$$

Here P and $\boldsymbol{u}$ are the average pressure and velocity in the mixture, ρ_L and c_L are the (undisturbed) density and speed of sound of the pure liquid, n is the number of bubbles per unit volume, and R is their radius. These two equations express respectively the conservation of mass and momentum in the mixture. It should be noted that, in (1), $R=R(\boldsymbol{x},t)$ must be understood as a field variable. This equation has been written assuming that all the bubbles in a macroscopic volume element surrounding $\boldsymbol{x}$ have the same radius. Extensions to mixtures of different sizes are straightforward in principle, although the added computational requirement would be significant. For this reason here we only consider bubbles having the same undisturbed radius. Caflisch *et al.* (1985) show that (1) and (2) have an error $o(\beta)$, where β is the gas volume fraction given by

$$\beta=\tfrac{4}{3}\pi R^3 n. \tag{3}$$

In view of the fact (shown in §6 below) that variations in n are $O(\beta)$, (1) can also be written, to the same accuracy, as

$$\frac{1}{\rho_L c_L^2}\frac{\partial P}{\partial t}+\nabla\cdot\boldsymbol{u}=\frac{\partial \beta}{\partial t}. \tag{4}$$

An important point about the previous model that should be explicitly noted is the fact that, in spite of their superficial appearance, the equations have not been linearized. The right-hand sides of (1) or (4) are to be regarded as genuinely nonlinear so that the model is applicable, in the dilute limit, also to nonlinear waves. This point can be made clearer by the following qualitative argument. Consider a one-dimensional situation with the bubbly liquid occupying a tube of cross-sectional area S and let a piston execute oscillatory motion with amplitude A and frequency ω. The volume swept by the piston is of the order of SA and, neglecting liquid compressibility, this volume must equal the combined volume change of the bubbles. Since the speed of signals c_m in the mixture is finite, the only bubbles that can participate are those within a distance of the order of the wavelength $\Lambda \sim c_m/\omega$ from the piston. Their number is of the order of $n\Lambda S$ and, if each one of them undergoes a volume change Δv, we must have

$$AS \sim n\Lambda S \Delta v, \tag{5}$$

from which, with $\Delta v \sim R^2 \Delta R$,

$$A/\Lambda \sim \beta \Delta R/R, \tag{6}$$

and also, since $u \sim A\omega$,

$$u/c_m \sim \beta \Delta R/R. \tag{7}$$

This argument, which contains the essential physics of the more formal scaling analysis presented by Caflisch *et al.*, shows that, for small β, even large-amplitude bubble motions only result in a small-amplitude motion of the mixture as a whole.

The analysis of Caflisch *et al.* also shows that the radius R appearing in (1) must be determined from the radial equation of motion for an isolated bubble immersed in the ambient pressure field P. Here we use the Keller equation (Keller & Kolodner 1956; Keller & Miksis 1980; Prosperetti & Lezzi 1986) that includes in an aproximate way the effects of liquid compressibility:

$$\left(1-\frac{1}{c_L}\frac{\partial R}{\partial t}\right)R\frac{\partial^2 R}{\partial t^2}+\frac{3}{2}\left(1-\frac{1}{3c_L}\frac{\partial R}{\partial t}\right)\left(\frac{\partial R}{\partial t}\right)^2=\frac{1}{\rho_L}\left(1+\frac{1}{c_L}\frac{\partial R}{\partial t}+\frac{R}{c_L}\frac{\partial}{\partial t}\right)(p_B-P). \tag{8}$$

The pressure in the liquid at the bubble surface p_B is related to the internal gas pressure p by the balance of normal stresses across the bubble interface

$$p = p_B+\frac{2\sigma}{R}+\frac{4\mu_L}{R}\frac{\partial R}{\partial t}, \tag{9}$$

where σ and μ_L are the surface tension and liquid viscosity. At normal pressures and for liquids far from the boiling point, such as water at room temperature, the partial pressure of the vapour is very small and can be neglected so that p in (9) may be taken to be just the gas pressure. It is clear that (8) reduces to the Rayleigh–Plesset equation in the incompressible limit $c_L \to \infty$. In equilibrium conditions (index a) (8) and (9) show that the bubble internal pressure is given by

$$p_a = P_a+2\sigma/R_a. \tag{10}$$

It has been shown by Nigmatulin and co-workers (Nigmatulin & Khabeev 1974, 1977; Nagiev & Khabeev 1979; Nigmatulin, Khabeev & Nagiev 1981) that, with the assumptions of spatial uniformity of the pressure and perfect nature of the gas, one has

$$\frac{\partial p}{\partial t} = \frac{3}{R}\left[(\gamma-1)K\frac{\partial T}{\partial r}\bigg|_{r=R}-\gamma p\frac{\partial R}{\partial t}\right], \tag{11}$$

where K and γ are the gas thermal conductivity and ratio of specific heats. The temperature field T in the gas is obtained from the energy equation that, with the previous assumptions, becomes (see e.g. Prosperetti, Crum & Commander 1988)

$$\frac{\gamma}{\gamma-1}\frac{p}{T}\left\{\frac{\partial T}{\partial t}+\frac{1}{\gamma p}\left[(\gamma-1)K\frac{\partial T}{\partial r}-\tfrac{1}{3}r\frac{\partial p}{\partial t}\right]\frac{\partial T}{\partial r}\right\}-\frac{\partial p}{\partial t}=\nabla\cdot(K\nabla T). \tag{12}$$

In (11) and (12) r is the radial coordinate measured from the centre of the bubble. It may be noted that, in addition to r and t, T also depends on the location x of the centre of the particular bubble being considered. It has been shown in Prosperetti *et al.* (1988) and in Kamath, Prosperetti & Egolfopoulos (1993) that the liquid temperature at the bubble wall remains substantially unaffected by the motion of the bubble. In other words, the specific heat of the liquid can be taken to be effectively infinite, so that consideration of the liquid temperature field is unnecessary.

Equation (11) can be recast in the form

$$\frac{\partial}{\partial t}(pR^{3\gamma})=3(\gamma-1)R^{3\gamma-1}K\frac{\partial T}{\partial r}\bigg|_{r=R}, \tag{13}$$

which shows that, in the absence of heat exchange at the bubble wall, the gas follows the adiabatic law. It will be clear from the following, however, that the right-hand side of this equation has a crucial effect on the propagation of pressure waves in bubbly liquids and apparently cannot be approximated in any simple way.

The numerical treatment of the previous model has been described in detail in Prosperetti & Kim (1987) and Kamath & Prosperetti (1989) for the unsteady one-dimensional problems considered below. The average equations (1) and (2) are discretized on a staggered finite-difference grid, while a spectral method is used for the energy equation in the gas at each station x. The procedure is second-order accurate both in space and in time. The standard tests of convergence were satisfactorily performed. As a further check, we have simulated the case shown in figure 6.4.5 of Nigmatulin (1991, vol. II, p. 40) finding excellent agreement. It was also explicitly verified that the solutions to the initial-value problem evolved into the steady waveforms calculated by the method of §4 below.

3. Unsteady one-dimensional shock waves

Before turning to the propagation of steady shock waves, which is the major focus of the present study, we look briefly at unsteady one-dimensional waves to point out the importance of a correct modelling of the gas thermo-fluid-dynamic behaviour.

The situation we model is typical of the experimental procedure used in the study of shock waves in bubbly liquids. The mixture is initially in equilibrium and at rest. The calculation is started at time $t=0$ with $P=P_a$ everywhere in the tube except in the immediate proximity of the boundary $x=0$. Here we set P equal to P_b at the first node and use a hyperbolic tangent profile to connect to P_a. We have varied the thickness of this initial transition layer from 2 to 20 computational cells and found a negligible effect except very near $x=0$. In particular, all the results shown below are insensitive to this starting condition. Here and in the following the subscripts a and b refer to conditions ahead of, and behind, the shock. The computational cells Δx are typically 10 mm long and the time step is such that $U\Delta t/\Delta x=0.25$, where U is the wave velocity.

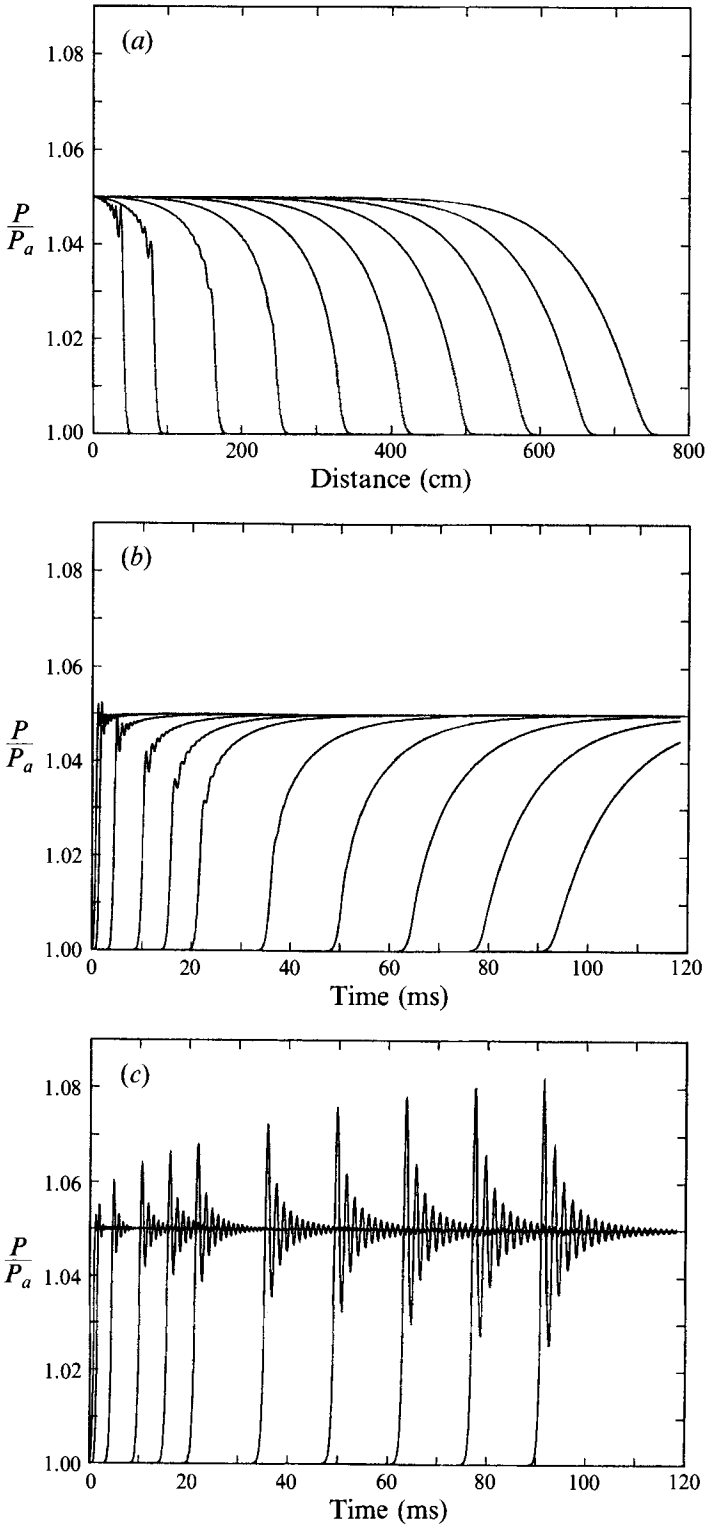

FIGURE 2. (*a*) Computed liquid pressure P non-dimensionalized by the pressure P_a ahead of the wave as a function of position at several instants of time for a shock wave in a water–glycerin mixture

We show in figure 2(*a*) the mixture pressure P as a function of position at several instants of time between 5.91 and 106.3 ms for $R_a = 1.18$ mm, $\beta_a = 2.94\%$ ($n_a = 4272$ m^{-3}), $P_b/P_a = 1.05$, $P_a = 0.123$ MPa. The physical properties are those of air at 20 °C in a 50% water–glycerin solution ($\gamma = 1.4$, $\mu_L = 7.88$ cP, $\rho_L = 1126$ kg m^{-3}, $c_L = 1481$ m s^{-1}). The pressure as a function of time at several positions between $x = 0.05$ and 6.5 m from the boundary located at $x = 0$ is shown in figure 2(*b*). The three different types of waveforms observed by Noordzij & van Wijngaarden (1974) and reproduced in figure 1 are evident here. Initially the wave is oscillatory with short periods and overshoots the level P_b. In Noordzij & van Wijngaarden's terminology, this is the *A*-type waveform. The last two to three profiles show instead a completely smooth and monotonic wave structure, the *C* type. In between we encounter intermediate profiles that exhibit fairly smooth oscillations. These profiles are labelled *B*-type.

Qualitatively, this evolution matches very well that found in the experiments of Noordzij & van Wijngaarden. Contrary to their conclusion, however, and as previously noted by Nigmatulin and co-workers, it is clear that it can also be found without introducing a relative motion between the liquid and the bubbles. We shall return to this point in greater detail in later sections.

It is interesting to compare the predictions of the model outlined in the previous section with those of the one obtained by replacing the pressure equation (11) by the simple polytropic law

$$\frac{p}{p_a}\left(\frac{R}{R_a}\right)^{3\kappa} = 1, \tag{14}$$

where κ is the polytropic index. The same case as figure 2(*b*) simulated by using this relation with $\kappa = 1$ is shown in figure 2(*c*). The progression from *A*- to *C*-type waves is suppressed by this crude modelling of the gas behaviour. Other values of κ produce qualitatively similar results (see also Tan & Bankoff 1984*a*).

Since in our numerical method we do not take any precaution against the numerically induced oscillations that often plague shock-wave calculations in compressible fluids (see e.g. Beam & Warming 1976; Sod 1978), one must guard against the possibility that the oscillatory structure in figure 2 is a numerical artifact. We have satisfied ourselves that these oscillations are correct by repeating the calculations with several different values of the space and time steps, to which the numerically induced oscillations are sensitive.

It should be remarked that not all shocks evolve all the way from *A* to *C* type. In the study of steady shocks that will be described in the following sections it will be seen that the present model predicts a steady state of the *C* type only for very weak waves. Stronger ones are found to settle down to a *B* type. We have encountered steady shocks of the *A* type only in the case of very small bubbles that behave very nearly isothermally. This feature renders the simple model (14) fairly accurate, and one can therefore expect a behaviour similar to that shown in figure 2(*c*) in this case.

For other than very weak shocks, the transition from *A* to *B* and possibly *C* can take

containing air bubbles. The gas volume fraction is $\beta = 2.94\%$, the pressure ratio $P_b/P_a = 1.05$, the pressure ahead of the wave $P_a = 0.123$ MPa, and the bubble radius $R_a = 1.18$ mm. The wave is shown at times 5.908, 11.82, 23.63, 35.45, 47.26, 59.08, 70.90, 82.71, 94.53, and 106.3 ms after the initiation of the shock. (*b*) Liquid pressure as a function of time at several positions for the same shock as (*a*). The traces shown are at distances of 0.050, 0.30, 0.70, 1.1, 1.5, 2.5, 3.5, 4.5, 5.5 and 6.5 m from the boundary of the gas–liquid mixture. (*c*) The same case as (*b*) but simulated with the isothermal pressure–volume relation for the gas contained in the bubbles. Note the drastic alteration of the waveforms.

quite some distance and our analysis suggests that many of the experimental results presented in the literature as steady shocks correspond in fact to still-evolving waves.

4. Steady waves

Consider one-dimensional waves of permanent form propagating from right to left with constant velocity U so that in all the previous relations $\partial/\partial t \to U\partial/\partial x$. The bubble number density n is a constant throughout the system. Ahead of the wave (subscript a) the mixture velocity vanishes, while the pressure, volume fraction, and bubble radius are P_a, β_a, and R_a. Upon integration of (4) we thus find

$$u/U = (P_a - P)/(\rho_L c_L^2) + \beta - \beta_a, \tag{15}$$

and, upon integration of (2),

$$\rho_L U u + P = P_a. \tag{16}$$

After elimination of the mixture velocity u we have

$$(1 - U^2/c_L^2)(P - P_a) + \rho_L U^2(\beta - \beta_a) = 0, \tag{17}$$

which, substituted into (15), gives

$$u/U = (1 - U^2/c_L^2)^{-1}(\beta - \beta_a). \tag{18}$$

This relation explicitly shows the mixture velocity to be a quantity of order β. This circumstance justifies the use in (2) of ρ_L in place of the mixture density, the difference being a quantity of order β.

Behind the wave (index b) the pressure is P_b, the radius R_b, and the volume fraction $\beta_b = \frac{4}{3}\pi R_b^3 n$. Inserting these values in (17) we find

$$\frac{U^2}{c_L^2} = \frac{P_b - P_a}{P_b - P_a - \rho_L c_L^2(\beta_b - \beta_a)}. \tag{19}$$

Since after the passage of the wave the bubbles are again in equilibrium and at the same temperature as the liquid, we have

$$(P_a + 2\sigma/R_a) R_a^3 = (P_b + 2\sigma/R_b) R_b^3. \tag{20}$$

For given conditions upstream of the wave, with this relation, the wave velocity U can be expressed solely in terms of the downstream pressure P_b. For negligible surface tension effects, the explicit expression is

$$\frac{U^2}{c_L^2} = \frac{P_b}{\rho_L c_L^2 \beta_a + P_b} = \frac{P_a}{\rho_L c_L^2 \beta_b + P_a}. \tag{21}$$

Unless β_a and β_b are extremely small, the second term in each denominator is much smaller than the first one so that

$$\frac{U^2}{c_L^2} \approx \frac{P_b}{\rho_L c_L^2 \beta_a} \approx \frac{P_a}{\rho_L c_L^2 \beta_b}. \tag{22}$$

Up to a term of order β^2, the first expression coincides with that given by Campbell & Pitcher (1958) for isothermal bubble behaviour. In the linear case $P_b - P_a \ll P_a$, (22) reduces to the well-known low-frequency result (see e.g. van Wijngaarden 1972)

$$U^2 = P_a/(\rho_L \beta_a). \tag{23}$$

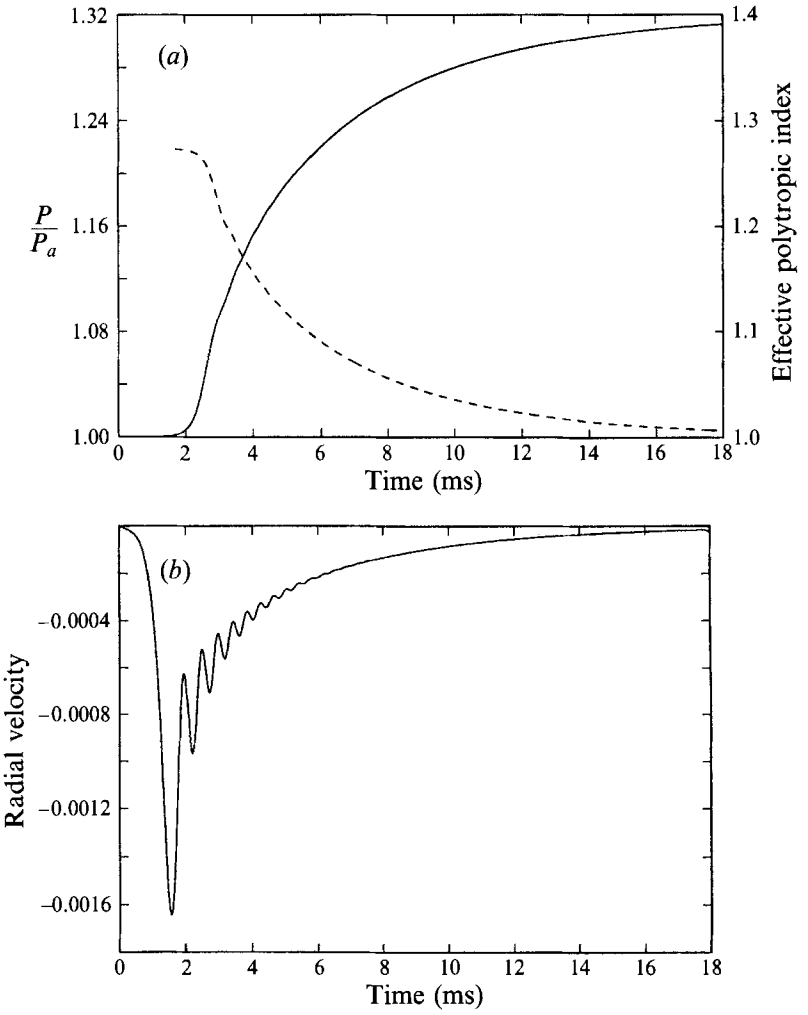

FIGURE 3. Example of a computed steady *B*-type waveform for $P_b/P_a = 1.32$, $\beta = 1\,\%$, $P_a = 0.1$ MPa, $R_a = 0.8$ mm. The graphs are in terms of a dimensional time defined by x/U, with the steady shock speed $U = 108$ m s^{-1} as obtained from (21). The oscillations of the wavefront are not very marked in (*a*), showing the liquid pressure, but they are very clear in (*b*), showing the bubble radial velocity. The dashed line in (*a*) (right vertical scale) is the effective polytropic index defined by (29).

With U determined from (19), (17) gives the pressure field throughout the wave in terms of the volume fraction or, since n is a constant to the present approximation, in terms of the local bubble radius, as

$$P = P_a + \frac{(P_b - P_a)(1-\beta/\beta_a)(P_b + 2\sigma/R_b)}{P_b - P_a + 2\sigma(1/R_b - 1/R_a)}. \tag{24}$$

With the neglect of surface tension effects, this relation becomes

$$P \approx P_a + P_b(1-\beta/\beta_a). \tag{25}$$

The problem is therefore reduced to the integration of the radial equation (8) which, with primes denoting differentiation with respect to x, may be written

$$\left(1-\frac{U}{c_L}R'\right)RR'' + \frac{3}{2}\left(1-\frac{U}{3c_L}R'\right)R'^2 = \frac{1}{\rho_L U^2}\left(1+\frac{U}{c_L}R' + \frac{R}{c}\frac{\partial}{\partial x}\right)(p_B - P), \tag{26}$$

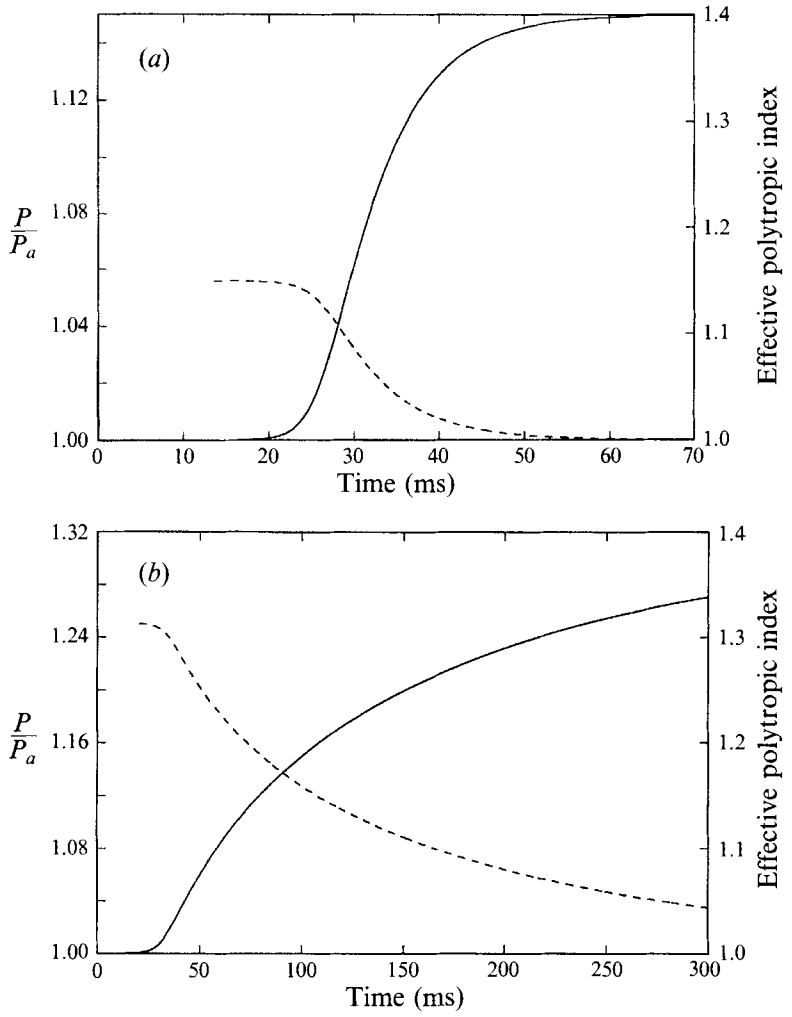

FIGURE 4. Example of a computed steady C-type waveform. (a) The parameter values are as for figure 3 except that the wave strength is $P_b/P_a = 1.15$. Here the shock wave speed is $U = 101$ m s^{-1}. (b) The parameter values are as for figure 3 except that the bubble radius is $R_a = 5$ mm. Here the shock wave speed is $U = 108$ m s^{-1}. The dashed line in (a) and (b) (right vertical scale) is the effective polytropic index defined by (29).

with p_B given by (9) and P by (24). The internal pressure p must of course be determined from the steady form of (11), i.e.

$$Up' = \frac{3}{R}\left[(\gamma-1)K\frac{\partial T}{\partial r}\bigg|_{r=R} - \gamma p U R'\right], \tag{27}$$

after integration of the energy equation

$$\frac{\gamma}{\gamma-1}\frac{p}{T}\left\{U\frac{\partial T}{\partial x}+\frac{1}{\gamma p}\left[(\gamma-1)K\frac{\partial T}{\partial r}-\tfrac{1}{3}rUp'\right]\frac{\partial T}{\partial r}\right\} - Up' = \nabla\cdot(K\nabla T). \tag{28}$$

Before turning to an analysis of the structure of the shock waves according to this model we show some examples, all computed with the same values of the physical properties used for figures 2(a) and 2(b). Figure 3 is a steady wave profile of the B type, which is found for $P_b/P_a = 1.32$, $\beta = 1\%$, $R_a = 0.8$ mm, $P_a = 0.1$ MPa. The natural

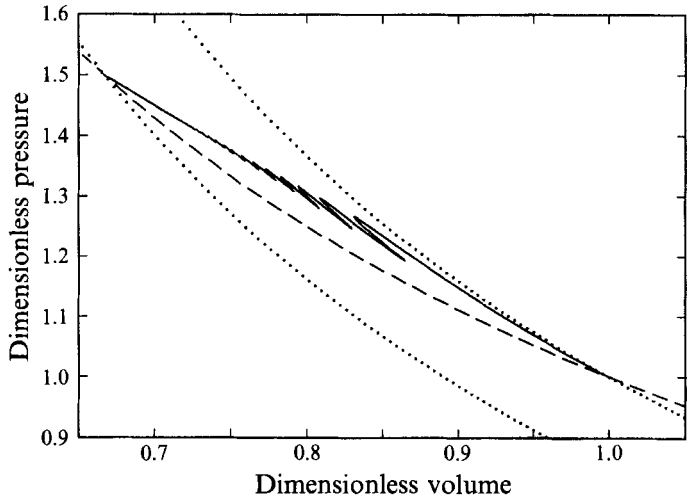

FIGURE 5. Bubble pressure–volume relation for a *B*-type shock with $R_a = 1$ mm, $P_a = 0.1$ MPa, $P_b/P_a = 1.5$, $\beta = 1\,\%$ (solid line). The dashed line is for an isothermal compression of the bubble as it traverses the wave, while the dotted lines indicate the adiabatic relation based on conditions ahead of the wave (upper line) and behind the wave (lower line). The steady wave profile for this case is shown in figure 12.

frequencies of the bubbles upstream and downstream of the wave are 3.78 and 4.25 kHz respectively. The graph is in terms of a dimensional time defined by x/U, with $U = 108\ \mathrm{m\,s^{-1}}$ in this case. The oscillations of the wavefront are not very marked in figure 3(*a*), showing the liquid pressure, but they become very clear if the bubble radial velocity along the wave is plotted, as in figure 3(*b*). This wave can be modified to assume a *C*-type waveform either by decreasing the shock strength, as in figure 4(*a*) ($P_b/P_a = 1.15$, $\beta = 1\,\%$, $P_a = 0.1$ MPa, $R_a = 0.8$ mm, natural frequencies 3.78 and 4.78 kHz, $U = 101\ \mathrm{m\,s^{-1}}$), or by increasing the bubble radius as in figure 4(*b*) ($P_b/P_a = 1.32$, $\beta = 1\,\%$, $P_a = 0.1$ MPa, $R_a = 5$ mm, natural frequencies 0.611 and 0.770 kHz, $U = 108\ \mathrm{m\,s^{-1}}$). We shall return to an explanation of these differences in the next section. Further examples of *B*-type waves are shown in figures 12 and 14.

An interesting insight into the thermal behaviour of the bubbles as they traverse the wave can be gained by defining an 'effective' polytropic index κ_e reversing (14), i.e.

$$\kappa_e = -\frac{1}{3}\frac{\log(p/p_a)}{\log(R/R_a)}. \tag{29}$$

This quantity, which represents the value of the polytropic index that would be needed to reproduce the instantaneous computed values of p and R, is shown by the dashed lines in figures 3 and 4. The range of variation of κ_e is quite wide and there is little hope of obtaining a realistic behaviour of the wave with a single value for this quantity.

The solid line in figure 5 illustrates the pressure–volume relation for a *B*-type shock with $R_a = 1$ mm, $P_a = 0.1$ MPa, $P_b/P_a = 1.5$, $\beta = 1\,\%$. (The wave profile for this case is shown in figure 12.) The dashed line corresponds to isothermal compression from upstream to downstream conditions, and the two dotted lines are the adiabatic relations based on the initial and final states. If one writes a polytropic relation based on the state upstream of the wave, as in (29), it is clear that the actual process is intermediate between isothermal and adiabatic so that $1 < \kappa_e < \gamma$ as in figures 3 and

4. If, however, one were to base a polytropic relation on the downstream state, the actual process would be outside the region bounded by the adiabatic and isothermal lines and one would thus need a polytropic index of less than 1 to reproduce the correct pressure–volume curve. To clarify this point note that, from the equation of state of perfect gases, one may write $pV^\kappa = N\mathscr{R}TV^{\kappa-1}$, with V the bubble volume, N the number of moles, and $\mathscr{R}$ the universal gas constant. If $\kappa > 1$ and the bubble is compressed, T has to increase in order for pV^κ to remain constant. This is the normal behaviour. However, if $\kappa < 1$, T decreases upon a compression. This is what must happen near the back of the wave where the bubbles, heated by compression in the first part of the wave, cool off by conduction and are further compressed to their final equilibrium radius behind the wave. These considerations are confirmed by the analysis that follows.

4.1. *Simplified models*

The main features of our results are unchanged by omitting the compressibility of the liquid and surface tension effects. Hence, for simplicity, in the asymptotic study of the front and back of the wave that follows, we shall use the Rayleigh–Plesset equation, rather than Keller's, with the average pressure P given by (25) so that

$$\rho_L U^2(RR'' + \tfrac{3}{2}R'^2) = p - \frac{4\mu_L U}{R}R' - P_a - P_b\left(1 - \frac{R^3}{R_a^3}\right). \tag{30}$$

For the purpose of comparing with earlier results, we also write the corresponding equation that would hold in the case of polytropic gas behaviour, (14), and constant effective damping μ_e analogous to the viscous damping, namely

$$\rho_L U^2(RR'' + \tfrac{3}{2}R'^2) = P_a\left(\frac{R}{R_a}\right)^{3\kappa} - \frac{4\mu_e U}{R}R' - P_a - P_b\left(1 - \frac{R^3}{R_a^3}\right). \tag{31}$$

4.2. *The shock front*

To study the behaviour of the shock front, following van Wijngaarden (1970), we let

$$R = R_a(1+X), \quad p = P_a(1+q). \tag{32}$$

In the second expression we write P_a in place of p_a consistently with the neglect of surface tension effects (cf. (10)). Upon linearization of (30) or (31) about R_a, P_a one finds

$$\rho_L U^2 R_a^2 X'' = P_a q - 4\mu_L U X' + 3P_b X. \tag{33}$$

In the polytropic case q is given by

$$q = -3\kappa X, \tag{34}$$

and the radial equation has solutions of the form

$$X \propto \exp \lambda_a x, \tag{35}$$

with

$$U\lambda_a = -b_{v,e} + \left[b_{v,e}^2 + \frac{3P_a}{\rho_L R_a^2}\left(\frac{P_b}{P_a} - \kappa\right)\right]^{1/2}, \tag{36}$$

where $b_{v,e}$ is the viscous damping parameter

$$b_v = 2\mu_L/(\rho_L R_a^2), \tag{37}$$

evaluated in correspondence of the effective viscosity μ_e rather than μ_L and based on the bubble radius ahead of the wave (see e.g. Devin 1959; Plesset & Prosperetti 1977;

Prosperetti 1991). For a wave progressing from right to left all disturbances must tend to zero as $x \to -\infty$ so that it is necessary that $\mathrm{Re}\,\lambda_a > 0$ for a physically acceptable solution to exist. Clearly this is only possible if $P_b/P_a > \kappa$ which, for any value $\kappa > 1$, imposes unphysical restrictions on the strength of the wave. The only possibility is therefore $\kappa = 1$, i.e. isothermal behaviour (van Wijngaarden 1970). This conclusion however, is also unsatisfactory, as one would expect the bubble behaviour to depend on the shock strength although, in the framework of the polytropic model, no such dependence is available.

It is not possible to obtain a closed-form expression for the pressure correction q according to the complex model of (11) and (12). However, if a solution is sought by means of the Fourier transform (understood in the sense of generalized functions), the result is that the product of a (single-valued) function of the conjugate variable times the transform of X equals zero. This implies that the transform of X is a linear combination of delta distributions centred at the zeros of that function, so that X itself must be a linear combination of exponentials. This argument justifies looking for solutions of (33) of the same form (35) as for the polytropic model. In this way we find the following equation for the auxiliary dimensionless quantity $\Omega = (R_a^2 U\lambda_a/\chi)^{1/2}$:

$$\Omega^4 + \frac{4\nu_L}{\chi}\Omega^2 + \frac{3P_a R_a^2}{\rho_L \chi^2}\left[\kappa_a(\Omega) - \frac{P_b}{P_a}\right] = 0, \tag{38}$$

where $\nu_L = \mu_L/\rho_L$, and $\kappa_a(\Omega) = \dfrac{\gamma\Omega^2}{\Omega^2 + 3(\gamma-1)(\Omega\coth\Omega - 1)}$ (39)

has essentially the meaning of an 'equivalent' polytropic index. In these relations χ denotes the thermal diffusivity of the gas. The characteristic equation (38) coincides with that given by Nigmatulin (1991, p. 49, vol. II) aside from the – usually small – viscous contribution that was not included in that work. If the bubble radius is not too small, the fraction multiplying the square bracket is large so that κ_a is close to P_b/P_a, at least as long as $P_b/P_a \leqslant \gamma$.

As before, only roots such that $\mathrm{Re}\,\lambda_a > 0$ are acceptable. Approximate solutions of (38) are readily found for small and large values of the quantity Ω. In the first case one has

$$\kappa_a \approx 1 + \frac{\gamma-1}{15\gamma}\Omega^2, \tag{40}$$

so that $$U\lambda_a \approx -(b_v + b_{iso}) + \left[(b_v + b_{iso})^2 + \frac{3P_a}{R_a^2\rho_L}\left(\frac{P_b}{P_a} - 1\right)\right]^{1/2}, \tag{41}$$

where $$b_{iso} = \frac{\gamma-1}{10\gamma}\frac{P_a}{\rho_L\chi} \tag{42}$$

is the thermal damping parameter for nearly isothermal conditions (Prosperetti 1984, 1991) and b_v is as defined by (37) with the correct liquid viscosity μ_L. In view of the large numerical value of P_a, unless the bubble radius is exceedingly small (i.e. in most conditions of interest), $b_v \ll b_{iso}$. It is readily seen that, for Ω to be so small that this approximation is legitimate, P_b/P_a must be close to 1, i.e. the shock must be weak. It is interesting to note that the result (41) implies that, in this limit of weak shocks, X approximately satisfies the equation

$$\rho_L R_a^2 U^2 X'' = -3P_a X - 2(2\mu_L + \rho_L R_a^2 b_{iso}) UX' + 3P_b X. \tag{43}$$

Upon comparison with (33), (34), it is seen that the gas behaviour is approximately isothermal, in agreement with (40), but with a damping increased by the relatively large amount b_{iso}.

In the opposite limit of large values of Ω one readily finds

$$\kappa_a \approx \gamma, \tag{44}$$

so that

$$U\lambda_a \approx \left[b_v^2 + \frac{3P_a}{R_a^2 \rho_L}\left(\frac{P_b}{P_a} - \gamma\right)\right]^{1/2} - b_v, \tag{45}$$

and for this result to correspond to a large value of Ω with $\mathrm{Re}\,\lambda_a > 0$, it is necessary that $P_b/P_a > \gamma$, i.e. that the shock be (relatively) strong. The equation satisfied by X in this case is, in place of (43),

$$\rho_L R_a^2 U^2 X'' = -3\gamma P_a X - 4\mu_L U X' + 3P_b X. \tag{46}$$

This shows that thermal damping effects have become negligible and that the gas behaves adiabatically as implied by (44).

It may be shown by an application of the Nyquist criterion that (38) possesses only one acceptable root (Nigmatulin 1991, p. 50, vol. II) of which (41) and (45) are the limit values. All other roots have $\mathrm{Re}\,\lambda_a \leqslant 0$ and are therefore unphysical. As before, we thus find exponentially growing solutions near the shock front, but their behaviour conforms now much better to physical intuition.

It is also interesting to note that the value of κ_a given by (39) is in very close agreement with the initial constant value of the 'effective' polytropic index (29) determined numerically near the wave front and shown by the dashed lines in figures 3(*a*) and 4. The numerical values are 1.273, 1.149, and 1.313 in the three cases, and the corresponding ones given by (39) are 1.281, 1.149, and 1.315.

4.3. *The back of the shock*

We may proceed in a similar way to study the shock structure near the back. We let

$$R = R_b(1+X), \quad p = P_b(1+q). \tag{47}$$

For the polytropic model (31) the equation corresponding to (33) is

$$\rho_L U^2 R_b^2 X'' = -3\kappa P_b X - 4\mu_L U X' + 3P_a X, \tag{48}$$

from which, with $X \propto \exp(-\lambda_b x)$,

$$U\lambda_b = b_{v,e} \pm \left[b_{v,e}^2 + \frac{3P_a}{\rho_L R_b^2}\left(1 - \kappa\frac{P_b}{P_a}\right)\right]^{1/2}, \tag{49}$$

where $b_{v,e}$ is computed from (37) with R_b in place of R_a and μ_e in place of μ_L. The physical condition that the wave must leave behind a medium at rest requires that $\mathrm{Re}\,\lambda_b > 0$, and therefore both roots are acceptable. It is clear from this result that, with the polytropic model, the back of the wave may exhibit the oscillations typical of the *A*-type shock structure when $\mathrm{Im}\,\lambda_b \neq 0$, i.e. when

$$b_{v,e}^2 < \frac{3P_a}{\rho_L R_b^2}\left(\frac{\kappa P_b}{P_a} - 1\right), \tag{50}$$

which will be verified for sufficiently strong shocks. When this inequality is not satisfied, the back of the wave is smooth as for the *B*- or *C*-type shocks.

If the gas pressure is obtained from (11), (12) we find, in place of (38),

$$\Omega^4 - \frac{4\nu_L}{\chi}\Omega^2 + \frac{3P_b R_b^2}{\rho_L \chi^2}\left[\kappa_b(\Omega) - \frac{P_a}{P_b}\right] = 0, \tag{51}$$

where $\Omega = (R_b^2 U\lambda_b/\chi)^{1/2}$ and

$$\kappa_b(\Omega) = \frac{\gamma\Omega^2}{\Omega^2 - 3(\gamma-1)(\Omega\cot\Omega - 1)}. \tag{52}$$

The fraction multiplying the term in square brackets in (51) is usually quite large so that $\kappa_b \approx P_a/P_b$ and, hence, $\kappa_b < 1$. For the three examples of figures 3 and 4 the values of κ_b given by (51), (52) are 0.7575, 0.8695, 0.7575, respectively. Values obtained from the full computation on the basis of a relation similar to (29) with p_b, R_b in place of p_a, R_a are instead 0.767, 0.870, and 0.786. The values for the first and third example are very close since the pressure ratio is the same and the effect of bubble radius small.

For small Ω the approximation corresponding to (40) is

$$\kappa_b \approx 1 - \frac{\gamma-1}{15\gamma}\Omega^2, \tag{53}$$

and leads to

$$U\lambda_b \approx b_v + b_{iso} \pm \left[(b_v + b_{iso})^2 + \frac{3P_b}{R_b^2\rho_L}\left(1 - \frac{P_a}{P_b}\right)\right]^{1/2}, \tag{54}$$

where b_v and b_{iso} are given by (37), (42) with R_b, P_b in place of R_a, P_a. These two roots are always real. The condition for their existence is that Ω^2 be small, which will be the case provided P_b/P_a is close to 1, i.e. the shock is weak.

The characteristic equation (51) also possesses an infinity of other roots close to $N\pi$, with $N = 1, 2, \ldots$. Approximations to these roots may be obtained by substituting $\Omega = \pi N + \epsilon$ in (51), (52) to find, for $N \gg 1$,

$$\epsilon \approx 3\frac{\gamma-1}{\pi N}\left\{1 - \frac{3(\gamma^2-1)}{\pi^2 N^2} + 3\left[\tfrac{3}{5}(\gamma-1)^2(9\gamma^2+17\gamma+9) - \frac{\gamma P_b R_b^2}{\rho_L \chi^2}\right]\frac{1}{\pi^4 N^4}\right\}, \tag{55}$$

from which

$$\kappa_b \approx -(\pi N)^4 \frac{\rho_L \chi^2}{3P_b R_b^2}, \tag{56}$$

$$U\lambda_b = \frac{\chi}{R_b^2}\Omega^2 \approx \frac{\chi}{R_b^2}(N\pi)^2. \tag{57}$$

More interestingly, (51) also possesses a pair of complex roots. When their modulus is large, the argument is close to $\pm\frac{1}{4}\pi$ or $\pm\frac{3}{4}\pi$ so that one can approximately take $\cot\Omega \approx \mp i$ from which

$$U\lambda_b \approx \left(\frac{3P_b\chi^2}{\rho_L R_b^6}\right)^{1/4}\left[\frac{3}{2\sqrt{2}}\gamma(\gamma-1) \pm i\left(\gamma - \frac{P_a}{P_b}\right)^{1/2}\left(\frac{3R_b^2 P_b}{\rho_L\chi^2}\right)^{1/4}\right]. \tag{58}$$

These roots are of particular interest since they appear to be the only ones capable of conferring an A-type structure to the back of the wave. For this to happen $\mathrm{Re}\,\lambda_b$ must be small so that attenuation is not excessive and this asymptotic formula is not applicable. However, it does indicate the potential presence of oscillatory solutions and indeed we have found numerically that a prominent oscillatory structure near the back of the wave appears for small bubbles as will be discussed in the next section. In this

case, the wavelength of the oscillation found numerically is quite close to that determined from the complex roots of (51).

5. *A*-, *B*-, and *C*-type steady shocks

We now turn to a consideration of the phase and group velocity of linear waves in a bubbly liquid according to the present model. This will afford some insight into the wave structure. Further details on the linear problem according to the present model may be found in Commander & Prosperetti (1989) and Lu & Prosperetti (1994).

Upon linearization of the model equations presented in §2, for perturbations proportional to $\exp \mathrm{i}(\omega t - kx)$, it is easy to obtain the following dispersion relation (Commander & Prosperetti 1989):

$$k^2 = \frac{\omega^2}{c_L^2} + \frac{4\pi\omega^2 R_e n}{\omega_0^2 - \omega^2 + 2\mathrm{i}b\omega}, \tag{59}$$

where the index e is used to denote equilibrium conditions. For the complete model the effective resonance frequency ω_0 and damping parameter b are given by

$$\omega_0^2 = \frac{p_e}{\rho_L R_e^2}\left(\operatorname{Re}\Phi - \frac{2\sigma}{R_e p_e}\right), \tag{60}$$

$$b = \frac{2\mu_L}{\rho_L R_e^2} + \frac{\omega^2 R_e}{2c_L} + \frac{p_e}{2\rho_L R_e^2 \omega}\operatorname{Im}\Phi, \tag{61}$$

where

$$\Phi = \frac{3\gamma}{1 - 3(\gamma-1)\mathrm{i}D[(\mathrm{i}/D)^{1/2}\coth(\mathrm{i}/D)^{1/2} - 1]}, \tag{62}$$

with

$$D = \chi/(\omega R_e^2), \tag{63}$$

the square of the ratio between the diffusion length and the bubble radius. For the polytropic model the dispersion relation has the same form (59), but ω_0 is given by

$$\omega_0^2 = 3\kappa p_e/(\rho_L R_e^2), \tag{64}$$

and the last term in b, representing the damping due to thermal effects, is absent. These seemingly slight differences have a profound effect on the dispersion relation, particularly at the lower frequencies (i.e. below the bubble resonance frequency) of concern here.

In the presence of dissipative processes one may define (at least) two different phase velocities, one, $\omega/\operatorname{Re}k$, appropriate for the boundary-value (or signalling) problem, and one, $\operatorname{Re}\omega/k$, appropriate for the initial-value problem. Much below the natural frequency, however, the effects of damping are small and the two definitions lead to nearly indistinguishable results. We use here the first definition appropriate for the signalling problem which is more easily calculated.

A comparison of the phase velocity as given by the polytropic and complete dispersion relations in the low-frequency region is shown in figure 6 for which the parameters are those of the shock-front region of the example shown earlier in figure 3. Here the lower and upper dashed lines are the polytropic results for isothermal and adiabatic motion, and the solid line is the complete model. The polytropic results start nearly flat, and then decrease as the natural frequency is approached. Since the mixture is stiffer if the bubbles compress adiabatically, the adiabatic line is above the isothermal one. The complete model shows instead an increase of the phase velocity at first, a maximum, and a subsequent decrease as ω further approaches ω_0. This behaviour is

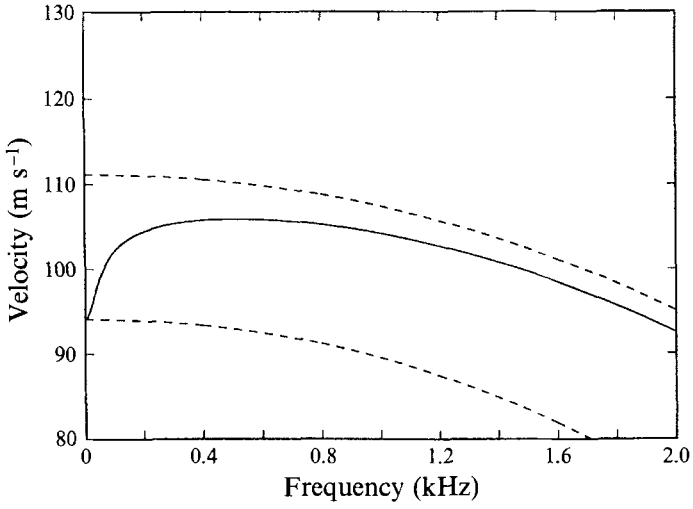

FIGURE 6. Comparison among the linear phase velocities as given by the complete (solid line), isothermal (lower dashed line), and adiabatic (upper dashed line) dispersion relations in the low-frequency region. The parameter values are those of the shock-front region of the example of figure 3, $P_a = 0.1$ MPa, $\beta = 1\,\%$, $R_a = 0.8$ mm.

quite interesting and can be readily explained as follows. At near-zero frequencies the bubbles behave isothermally. However, as the timescale of the motion shortens, heat cannot freely diffuse in and out of the bubble and the 'effective' polytropic index increases. The mixture then becomes stiffer and the phase velocity correspondingly increases toward the adiabatic result. The larger the bubbles, the closer they approach this adiabatic behaviour. At still higher values of ω, the presence of the resonance begins to become important: it is easier and easier to compress the mixture so that the stiffness goes down and with it the phase velocity.

It appears likely that the characteristic structure of the *B*-type wave is due to this rising and falling of the phase velocity at low frequencies and therefore cannot be captured by any simplified model that does not possess this characteristic. To illustrate this point we present figure 7, where we draw the phase V_p and group V_g velocities for the state of the mixture near the front and near the back of the waves of figures 3 and 4 together with a horizontal line representing the speed of the shock. The definitions of phase and group velocities used here are

$$\frac{1}{V_p} = \frac{\mathrm{Re}\, k}{\omega}, \quad \frac{1}{V_g} = \mathrm{Re}\frac{\mathrm{d}k}{\mathrm{d}\omega}, \tag{65}$$

and correspond therefore to the boundary-value problem, although the differences with the initial-value problem are minor as noted before. Figure 7(*a*) (corresponding to figure 3) is for a shock wave of the *B* type, and figures 7(*b*) and 7(*c*) (corresponding to figures 4(*a*) and 4(*b*) respectively) are for shock waves of the *C* type.

It is well known that in many cases diagrams similar to those displayed in these figures may be used to understand the structure of the front and back of shock waves (see e.g. Lighthill 1978). The points where the shock speed crosses the phase velocity lines correspond to sinusoidal wavelets propagating at the same speed as the shock. Wavelets with the corresponding frequency and wavenumber can therefore form a steady oscillatory pattern associated with the shock. If the shock dissipates energy exclusively by radiation, these wavelets can exist near the back only if the corresponding

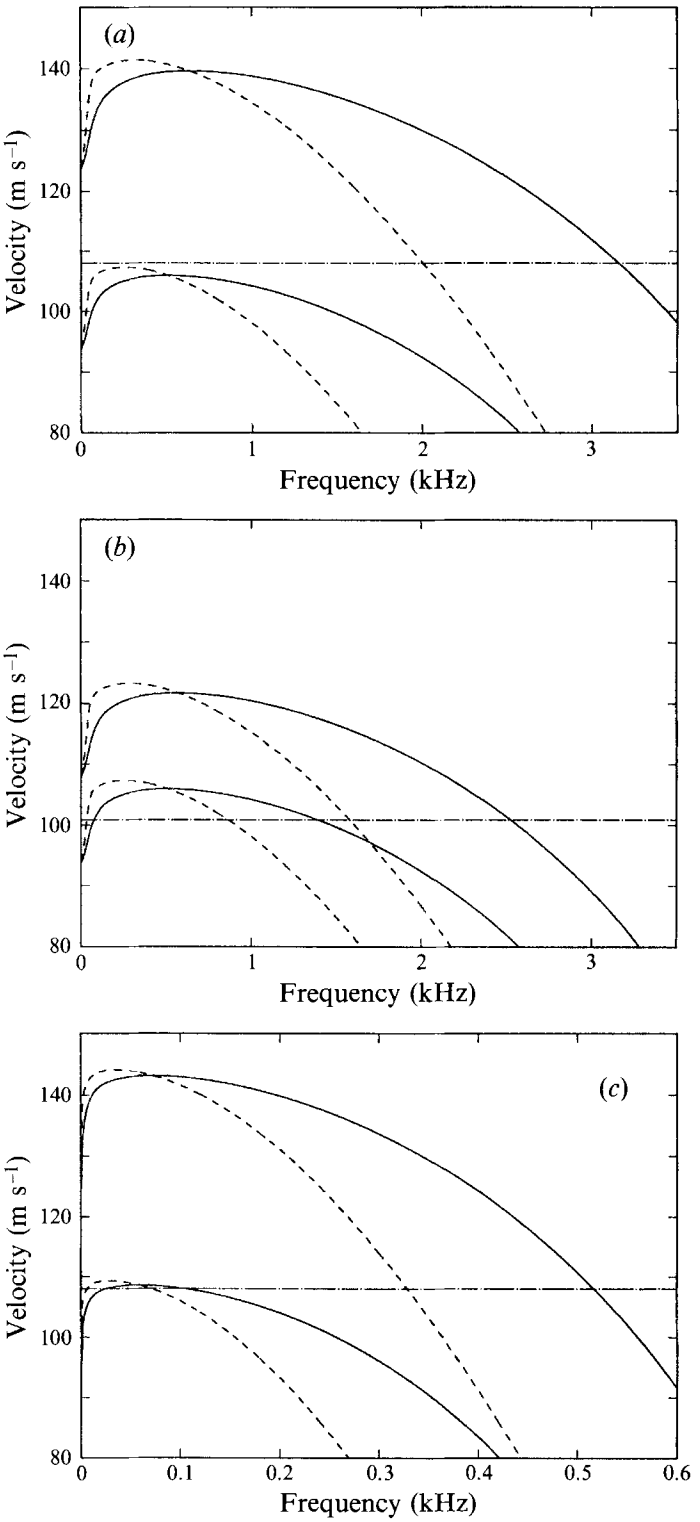

FIGURE 7. Phase (solid lines) and group (dashed lines) velocities for the state of the mixture near the front (lower pair of curves) and near the back (upper pair) of (*a*) the *B* shock of figure 3, (*b*) the *C* shock of figure 4(*a*), and (*c*) the *C* shock of figure 4(*b*), in the low-frequency region. The dash-and-dot line is the steady shock speed.

group velocity is smaller than the shock velocity (so that energy is left behind), and near the front only if the corresponding group velocity is greater than the shock velocity (so that the energy can propagate upstream into the undisturbed medium). This argument is not generally applicable in the presence of strong non-radiative dissipation mechanisms, which is the case of present interest: even if a pattern of steady wavelets is kinematically possible, the non-radiative dissipation of energy might be too strong for it to sustain itself. However, while this condition may not be a sufficient criterion for the presence of oscillatory structures associated with the shock, it clearly still remains necessary. From figures 7(*b*) and 7(*c*), corresponding to *C* shocks, we see that the conditions of the previous argument would be satisfied for very low frequencies (of the order of 75 and 25 Hz for these examples) ahead of the shock, and for higher frequencies (of the order of 2.53 and 0.517 kHz respectively) at the back. A close examination of the numerical results for these nonlinear steady shocks reveals however that no appreciable wave structure is present, a fact that is confirmed by the linear analysis of the previous section.

If we now consider the dispersion relations for the *B*-shock case of figure 3, shown in figure 7(*a*), we immediately recognize a major qualitative difference with the previous ones, namely the fact that the shock speed is always greater than the phase speed of the waves near its front. This explains the much steeper rise of the wave front found in this case as compared with the previous one (cf. figures 3 and 4*a*). Consider the regions with increasingly higher pressure that are encountered as one traverses the wave from the front to the back. Approximately the local state of the mixture in each one of these regions may be represented by a pair of phase and group velocity lines intermediate between the front and back ones shown in figure 7(*a*). For a certain value of the pressure, P_*, say, the phase velocity curve reaches a maximum value equal to the shock speed. Since phase and group velocities are equal at an extremal point of the former, for the portion of the wave where $P \approx P_*$, wavelets are possible for which both the phase and group velocities equal the shock velocity. These wavelets can therefore exist without losing energy due to radiation, and a *B*-type structure becomes possible. On the basis of this argument, we propose that the criterion for the transition between *C*- and *B*-type shocks is therefore

$$\max V_{p,\,front} = U. \tag{66}$$

When the maximum phase velocity of the wavelets near the shock's front is smaller than the shock velocity U, the shock is of the *B* type while, when it is greater, a *C* structure is encountered.

This hypothesis may be strengthened by a consideration of the transient process by which the shock becomes steady. In the typical experiments the initial perturbation is short, with a corresponding high-frequency content. In the *C* case, all these high-frequency wavelets either remain behind the shock or race ahead of it: the balance between nonlinearity and dispersion is essential to maintain the integrity of the wave, and the shock is thick. In the *B* case, on the other hand, no wavelets can escape from the front of the shock which is therefore thin with an appreciable high-frequency component.

These considerations may perhaps be put on a firmer quantitative footing by application of one of the several asymptotic techniques developed for the study of nonlinear waves (see e.g. Whitham 1974; Jeffrey & Kawahara 1982).

The criterion (66) for the existence of steady *B*- or *C*-type shocks cannot be put in a simple analytic form. However, with the neglect of surface tension and viscous effects and the use of suitable combinations of the variables, for each value of γ, it can be

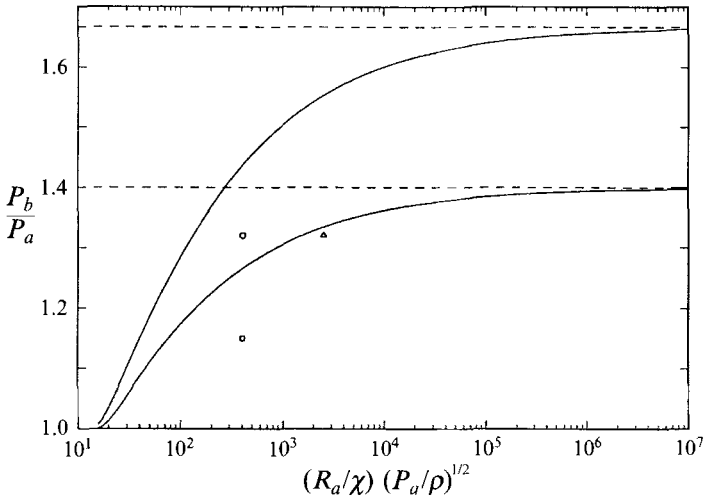

FIGURE 8. The boundary (66) between steady B- and C-type shocks for monatomic ($\gamma = \frac{5}{3}$, upper curve) and diatomic ($\gamma = \frac{7}{5}$, lower curve) gases. C shocks are found in the region below the curves and B shocks above. The circle, square, and triangle mark the cases shown in figures 3, 4(a) and 4(b) respectively. The dashed lines are for $P_b/P_a = \gamma$.

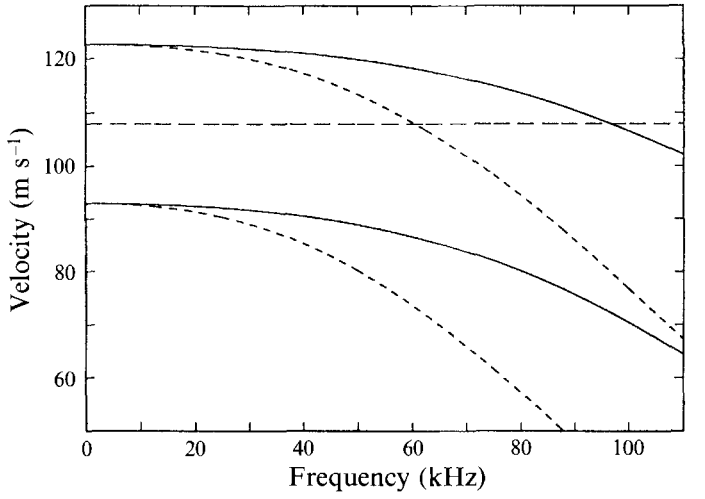

FIGURE 9. Typical phase (solid lines) and group (dashed lines) velocities for very small bubbles for which dissipative effects are very strong. The case shown here corresponds to $R_a = 20\ \mu$m, $P_a = 0.1$ MPa, $\beta = 1\%$.

represented by a single curve that we show in figure 8. The lower curve is for $\gamma = \frac{7}{5}$ (diatomic gases) and the upper one for $\gamma = \frac{5}{3}$ (monatomic gases). The region below these curves corresponds to C shocks, and the region above to B shocks. Since the maximum of the phase velocity curve is the highest for adiabatic bubble behaviour, which is approximated by large bubbles, these curves tend asymptotically to γ for large bubble radii. The criterion $P_b/P_a = \gamma$ for transition from B to C shocks, proposed by Nigmatulin & Shagapov (1974), is thus seen to be approximately valid for large bubbles. In figure 8 the example of figure 3 is marked by the circle, that of figure 4(a) by the square, and that of figure 4(b) by the triangle. It is seen that all these cases

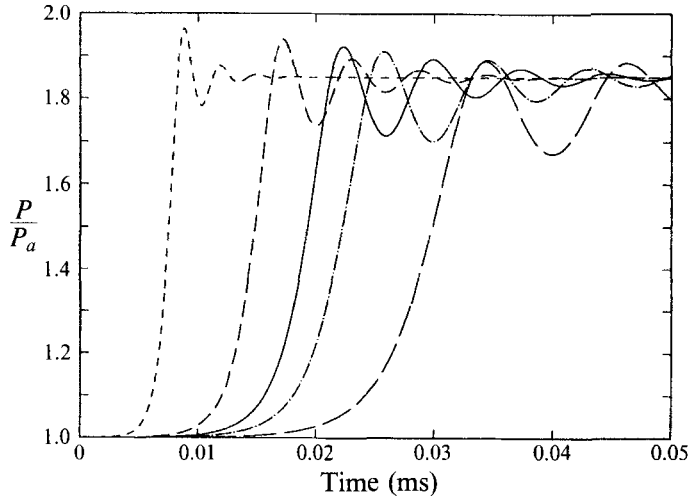

FIGURE 10. Examples of steady shock waves in a mixture containing very small bubbles with $P_b/P_a = 1.85$, $P_a = 0.1$ MPa, $\beta = 1\,\%$. The cases shown are, from the left, $R_a = 10$, 20, 26, 30 and 40 μm. Transition between the *A* and *B* type is estimated to occur at around 26 μm.

conform with the proposed criterion. We have encountered a similar favourable comparison in all the other cases that we have tested.

The mutual relationship between the phase and group velocities shown in figures 6 and 7 undergoes a marked qualitative change for very small bubble radii. An example is shown in figure 9 which refers to the case $P_b/P_a = 1.85$, $R_a = 20$ μm, $P_a = 0.1$ MPa, $\beta = 1\,\%$. Now dissipative effects are very pronounced and the group velocity does not increase in the neighbourhood of zero frequency, but starts decreasing immediately as for the polytropic case shown in figure 6. We thus expect an *A*-type shock structure to become possible in these conditions, as indeed is seen in the first two examples of figure 10 corresponding to $R_a = 10$ and 20 μm, $P_b/P_a = 1.85$, $P_a = 0.1$ MPa, $\beta = 1\,\%$. We have verified numerically that the wavelength of the oscillations visible in this figure is quite close to the complex root of (51) mentioned before. In this parameter range the quantity P_* previously defined ceases to exist.

On the basis of the preceding analysis, one may expect the transition between *B*- and *A*-type steady waves to take place when the second derivative of the group velocity evaluated at zero frequency vanishes. A quantitative expression of this criterion may be found from (59) from which we obtain

$$\left(3-\frac{2\sigma}{P_a R_a}\right)\left\{\left(\frac{\gamma-1}{5\gamma}\right)^2\frac{P_a R_a^2}{\rho_L \chi^2}+8\frac{\gamma-1}{5\gamma}\frac{\mu_L}{\rho_L \chi}+16\frac{\mu_L^2}{\rho_L P_a R_a^2}\right.$$
$$\left.+2\left(3-\frac{2\sigma}{P_a R_a}\right)\left[\frac{2(\gamma-1)(3\gamma+7)}{525\gamma^2}\frac{P_a R_a^2}{\rho_L \chi^2}-2\right]\right\}=0. \quad (67)$$

Shocks of the *B* type correspond to the quantity in the left-hand side being positive. The common factor $3-2\sigma/P_a R_a$ is positive for most cases of interest. This relation is only approximate insofar as it neglects liquid compressibility and the complex nature of the dispersion relation. It is shown in suitable non-dimensional variables in figure 11 for $\mu_L = 0$, where the circles correspond, from left to right, to the cases illustrated,

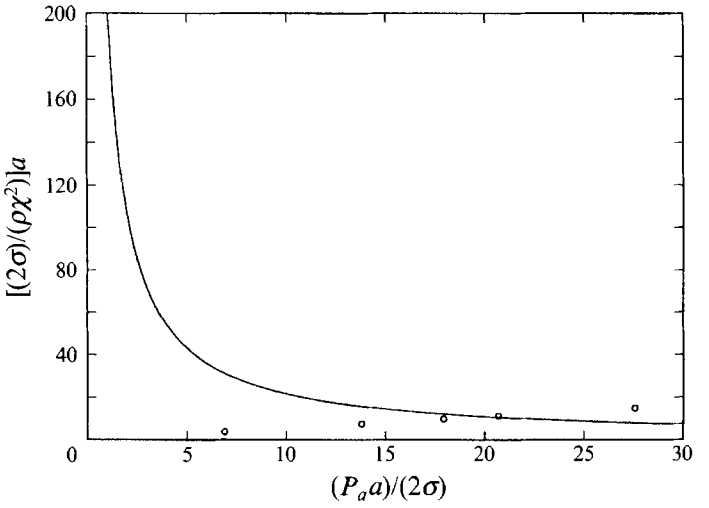

FIGURE 11. Boundary (67) between B-type (above the line) and A-type (below the line) steady shock waves. The circles correspond, from left to right, to the waveforms shown (from left to right) in figure 10.

in the same order, in figure 10. For $P_b/P_a = 1.85$, $P_a = 0.1$ MPa, $\beta = 1\,\%$, it gives $R_a \approx 28\,\mu$m. A direct solution of the zero-second-derivative condition leads to $R_a \approx 26\,\mu$m, again with the neglect of the imaginary part of the dispersion relation. According to the previous criterion, of the shock profiles of figure 10, the first two, corresponding to $R_a = 10$ and 20 μm should thus be of the A type and the last two, corresponding to $R_a = 30$ and 40 μm, of the B type. The first profile is clearly of the A type, while the case is less clear-cut for the following one. The proposed criterion is clearly not as precise as that for transition from B to C shocks, most likely because of the increased dissipative effects in this case.

6. Comparison with experiment

Detailed experimental data suitable for a test of the present theory are available in a thesis by Noordzij (1973). He used two vertical tubes with an inner diameter of 55 mm and lengths of 4.5 and 2.5 m. An air chamber above the bubbly liquid could be maintained at low pressure by means of a pump. To start the experiment a diaphragm separating the chamber from the atmosphere was broken, with a consequent abrupt rise of the pressure acting on the free surface of the mixture and the production of a shock. We provide in tables 1 and 2 comparisons between Noordzij's data and the results of the present model for the shock speed and the wavelength λ of the first oscillation of the A- and B-type shocks defined in figure 12. (This figure is the steady wave profile for the case $R_a = 1$ mm, $P_a = 0.1$ MPa, $P_b/P_a = 1.5$, $\beta = 1\,\%$. The quantity λ is similar to λ_b considered in §4.3 above, which however was defined as the wavelength of the oscillations near the back of the wave rather than near the front as here.)

In the tables the columns marked EXP show the data. Those with the heading UNST have been obtained by solving the unsteady problem up to the time necessary for the wave to reach the position at which the data were taken, while those marked ST correspond to steady waves. The difference between quantities in the last two columns gives a measure of the 'degree of unsteadiness' of the wave at the position at which the

Conditions					Results					
					Velocity (m s^{-1})			λ (mm)		
P_b/P_a	R_a (mm)	$P_a \times 10^{-5}$ (N m^{-2})	β_a (%)	x (m)	EXP	UNST	ST	EXP	UNST	ST
1.10	1.05	1.14	0.85	2.2	125	126.72	114.17	125	119.8	—
1.12	1.09	1.15	1.72	2.3	90	89.08	81.46	90	90.2	—
1.12	1.36	1.03	1.96	1.2	76	80.75	72.24	91	95.4	—
1.16	1.06	1.13	1.69	2.6	86	89.79	82.90	86	81.9	—
1.16	1.36	1.08	1.43	2.2	94	97.06	88.08	94	107.9	—
1.18	1.00	1.09	1.12	2.3	111	109.18	100.79	88	88.3	—
1.18	1.31	0.97	3.23	1.2	57	61.45	56.08	45	65.2	—
1.21	1.41	0.97	1.59	1.2	81	89.33	80.87	65	93.5	—
1.22	1.24	1.00	3.4	2.1	62	60.44	56.43	62	63.2	—
1.26	1.29	0.89	3.8	1.1	57	55.29	51.18	45	57.9	—
1.28	1.00	1.02	0.9	2.3	115	120.71	113.22	80	81.5	84.6
1.29	1.35	0.90	2.29	1.2	70	72.79	67.05	49	67.4	—
1.32	1.29	0.99	2.68	2.6	74	69.39	65.76	51	65.6	—
1.41	1.19	0.92	0.87	2.6	116	121.06	114.77	93	85.8	84.6
1.41	1.31	0.87	2.01	2.2	76	77.29	73.55	57	65.3	63.1
1.51	1.21	0.89	0.89	2.3	63	61.60	59.75	44	47.9	40.5
1.62	1.17	0.82	1.69	2.2	93	85.95	83.45	56	52.2	51.7
1.74	1.12	0.74	1.60	2.2	81	86.23	84.43	56	49.5	47.5
1.85	1.15	0.58	1.92	1.2	78	72.07	70.40	47	43.8	38.8
2.00	1.48	0.69	3.91	2.2	62	56.94	55.96	31	40.4	36.2
2.13	1.13	0.60	1.04	2.2	122	105.87	104.25	55	50.1	47.1
2.25	1.32	0.60	3.37	2.2	60	60.17	59.62	30	36.6	30.3
2.51	1.11	0.53	1.43	2.2	93	91.48	90.76	28	40.1	36.8
3.04	1.24	0.46	2.77	2.2	70	67.13	66.91	21	31.7	26.5
3.67	1.14	0.31	2.26	1.2	75	67.07	66.83	26	29.0	24.1
4.05	1.36	0.35	3.64	1.2	63	59.21	58.78	19	28.8	22.6

TABLE 1. The experimental results of Noordzij (1973) for *B* shocks are shown in the columns marked EXP. The columns bearing the headings UNST and ST show the numerical results for transient and steady shocks respectively.

Conditions					Results					
					Velocity (m s^{-1})			λ (mm)		
P_b/P_a	R_a (mm)	$P_a \times 10^{-5}$ (N m^{-2})	β_a (%)	x (m)	EXP	UNST	ST	EXP	UNST	ST
1.13	1.41	0.921	2.19	0.19	73	74.10	64.92	87	65.05	—
1.18	1.35	0.852	4.29	0.18	52	50.97	45.62	36	49.91	—
1.28	1.35	0.780	4.36	0.14	51	49.61	45.09	26	45.22	—
1.38	1.43	0.718	3.70	0.09	61	53.19	48.76	43	43.10	33.85
1.51	1.34	0.650	1.23	0.09	88	91.82	84.08	26	52.70	71.70
1.80	1.30	0.602	2.31	0.21	78	70.55	64.51	38	44.66	41.20
2.51	1.54	0.377	5.34	0.18	47	43.18	39.67	21	32.65	26.54
3.10	1.33	0.313	2.34	0.2	74	65.74	60.66	26	35.51	29.01

TABLE 2. The experimental results of Noordzij (1973) for *A* shocks. Column headings as for table 1.

data were taken. It is seen that the differences in wave speed are at most of the order of 10%, which is within the error band of much of the data. Table 1 gives results for *B*- and *C*-type shocks. For the latter ones, and for the marginal *B* cases, the quantity

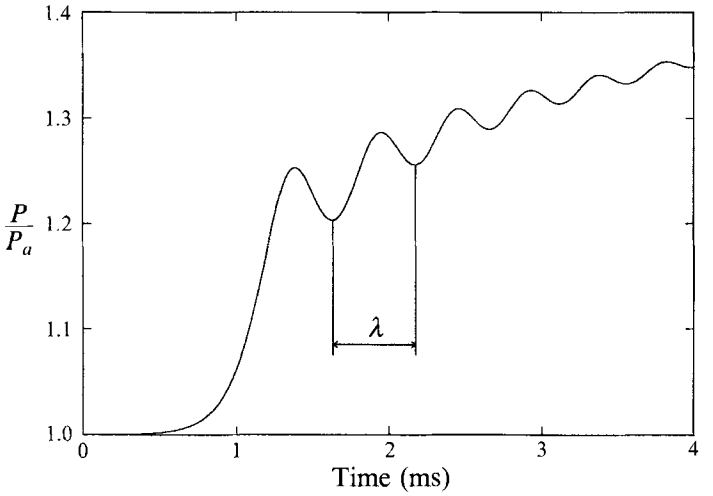

FIGURE 12. Definition of the quantity λ of tables 1 and 2. This figure is the steady wave profile for the case $P_b/P_a = 1.5$, $\beta = 1\,\%$, $R_a = 1$ mm, $P_a = 0.1$ MPa of figure 5.

λ is either undefined or too imprecisely determinable and the corresponding entry is blank. Of the A-type shocks, considered in table 2, the first two evolve to steady C type, the third one is borderline, and the remaining ones are of the B type.

In general a good agreement between theory and data can be observed in table 1, although differences are appreciable in a few cases. As λ depends also upon the shock velocity (see e.g. §4.3), it is not surprising that discrepancies are found for both quantities together. We have failed to find a systematic pattern among the cases of table 1 that agree or disagree with theory and experimental error may play a role. For the data of table 2 it appears that the comparison is worse the stronger the shock and the closer the measurement position to the boundary.

Noordzij's A-shock data were all taken within about 0.2 m from the surface of the bubbly liquid, a region where it is conceivable that the flow has an appreciable three-dimensional structure. The more recent set of data provided by Beylich & Gülhan (1990) is not subject to this objection. These authors have carried out an experimental study of shock waves using gases with strongly different values of γ: helium ($\gamma = \frac{5}{3}$), nitrogen ($\gamma = \frac{7}{5}$), and SF_6 ($\gamma \approx 1.09$). The region occupied by the bubbly liquid had a length of slightly less than 2 m, and they used shock strengths P_b/P_a of the order of 1.5–2. We compare the experimental wave profiles measured 0.975 m from the liquid free surface with the calculated ones in figure 13. It is clear that a significant discrepancy between theory and experiment exists. A striking difference – which is also encountered in some of the data of tables 1 and 2 – is between the computed and measured wavelengths. It may be pointed out that Beylich & Gülhan (1990) were only able to reconcile their model with the data by introducing a turbulent diffusivity more than 1000 times bigger than the molecular viscosity of their water–glycerin mixture.

FIGURE 13. The line with circles shows the data from Beylich & Gülhan for (*a*) helium bubbles (their figure 9, $P_a = 0.111$ MPa, $P_b/P_a = 1.78$, $R_a = 1.15$ mm, $\gamma = 1.67$, $\beta_a = 0.28\,\%$); (*b*) nitrogen bubbles (their figure 12, $P_a = 0.111$ MPa, $P_b/P_a = 1.57$, $R_a = 1.15$ mm, $\gamma = 1.4$, $\beta_a = 0.25\,\%$); (*c*) SF_6 bubbles (their figure 13, $P_a = 0.111$ MPa, $P_b/P_a = 1/81$, $R_a = 1.15$ mm, $\gamma = 1.09$, $\beta_a = 0.25\,\%$). The solid line is the predicted waveform according to the theory of §2. The dashed line is the predicted waveform including the gas–liquid relative motion effects according to the model of §6.

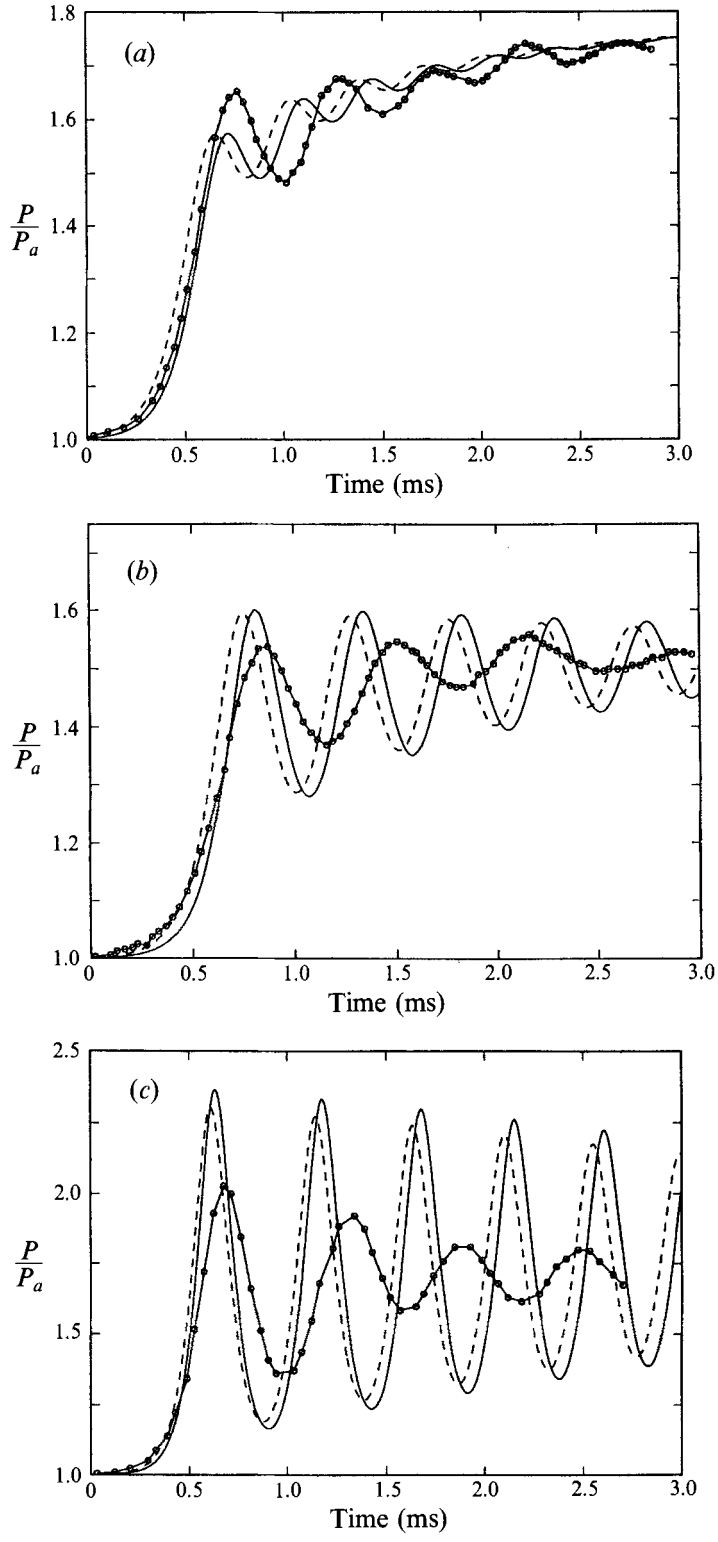

FIGURE 13. For caption see facing page.

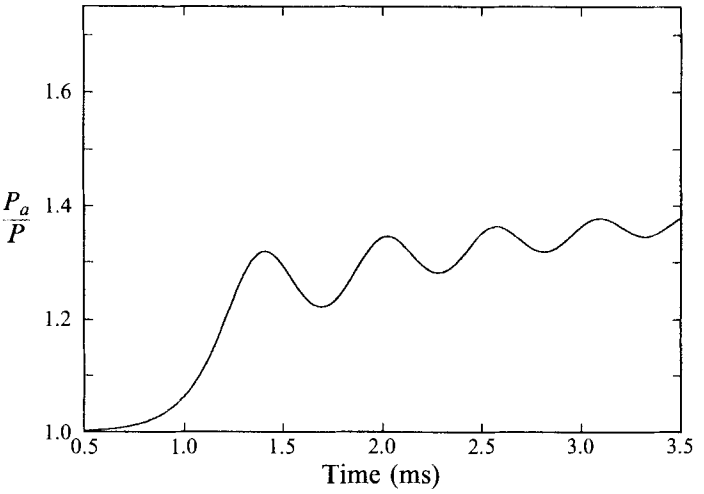

FIGURE 14. Computed steady waveform for the case of figure 13(*b*).

Figure 14 shows the steady profile for the nitrogen bubble case of figure 13(*b*). It is interesting to observe the increase of the oscillation period as the wave evolves, but the steady waveform does not seem to be any closer to the measurements than the transient one of figure 13(*b*). We simulated the propagation of this wave for over 8 m of travel distance and found that the waveform was still evolving and significantly different from the steady result of figure 14. This seems to indicate that the waves observed by Beylich & Gülhan were far from having reached steady conditions so that their application of the steady form of the theory to data reduction may not have been appropriate.

In order to investigate some possible sources of these differences we have combined the bubble dynamics model described in §2 with a more sophisticated formulation of the mixture behaviour, as follows. The usual form of the liquid continuity equation in averaged two-phase flow models is

$$\frac{\partial}{\partial t}[(1-\beta)\rho_L]+\nabla\cdot[(1-\beta)\rho_L \boldsymbol{u}_L] = 0. \tag{68}$$

Since the gas density is much smaller than the liquid density, the average liquid velocity $\boldsymbol{u}_L$ is very nearly equal to the average mixture velocity $\boldsymbol{u}$ in (1) and (2). In addition, $O(u) = O(\beta)$ (cf. (18)) and therefore, aside from the very small liquid compressibility effects, this equation coincides to $O(\beta)$ with the corresponding one, (1), used in the present model.

A standard (if approximate) form of the total momentum conservation for the mixture is

$$(1-\beta)\rho_L\left(\frac{\partial u}{\partial t}+u\frac{\partial u}{\partial x}\right) = -\frac{\partial P}{\partial x}. \tag{69}$$

Equations (68) and (69) coincide with the model used by van Wijngaarden (1968).

To close the model one needs a balance equation for the bubble number density n and for the bubble-field average velocity. For the first one we take the standard form

$$\frac{\partial n}{\partial t}+\nabla\cdot(n\boldsymbol{v}) = 0. \tag{70}$$

Since one expects $O(v) \sim O(u)$, this relation shows that variations in n are $O(\beta)$, as stated in §2.

Many different forms have been proposed for the equation for the relative motion. Here we use that of van Wijngaarden (1972) and Noordzij & van Wijngaarden (1974), namely

$$\rho_L\left[\left(\frac{\partial v}{\partial t}+v\frac{\partial v}{\partial x}\right)-\left(\frac{\partial u}{\partial t}+u\frac{\partial u}{\partial x}\right)\right]=-2\frac{\partial P}{\partial x}-18\frac{\mu_L}{R^2}(v-u). \tag{71}$$

The term on the left-hand side is proportional to the added mass of the bubble and the last one on the right-hand side accounts for the drag according to the high-Reynolds-number formula of Levich.

We have repeated the calculations of figure 13 using this more complex formulation for the mixture behaviour and the same model as before for the bubble dynamics. The results for the cases studied by Beylich & Gülhan (1990) are shown by the dashed lines in figure 13. Although the additional physical mechanisms contained in the more complex model – and primarily the phase slip – are of some importance, it is seen that their inclusion merely affects the phase of the oscillations, but not their period and does not therefore improve the comparison with the data. We have performed similar calculations for the examples with $\beta \sim 2\%$ of Beylich & Gülhan with similar conclusions.

One of the reviewers suggested using the speed of sound in the mixture (approximately given by (23)) rather than in the pure liquid in the Keller equation (8). We have tried this for the case of figure 13(*b*), finding an essentially equal wavelength with a slightly higher attenuation. The large discrepancy with the data remains.

7. Discussion of previous work

The results described in the previous sections throw an interesting light on previous research on this problem to a discussion of which we now turn.

The work conducted up to the early 1970s is summarized in van Wijngaarden (1972) and Noordzij & van Wijngaarden (1974). In the latter paper the existence of the three different wave profiles shown in figure 1 was reported, and it was pointed out that some type of relaxation process was necessary to account for them. Relative motion between the phases was introduced as a likely candidate, while the thermal behaviour of the bubbles was described by the simple polytropic relation (14). Although Noordzij & van Wijngaarden were able to demonstrate theoretically the existence of the three wave profiles observed in the experiments, agreement between their model and their data was at best inconclusive. The modelling of relative motion of Noordzij & van Wijngaarden was very similar to the one used before in §6, where its effect was shown to be small as also found by Nigmatulin (1982).

Another influential paper on shock waves in bubbly liquids was published at about the same time by Nigmatulin & Shagapov (1974) (see also Nigmatulin 1991). They seem to have been the first to realize that a relatively long time and propagation distance are necessary for the establishment of a steady wave profile which implied that this steady condition had not been reached in several of the available data. In their work the heat transfer between the gas and the liquid was modelled with a constant value of a Nusselt number defined by

$$Nu=-\frac{2R}{\langle T\rangle-T_\infty}\frac{\partial T}{\partial r}\bigg|_{r=R(t)}, \tag{72}$$

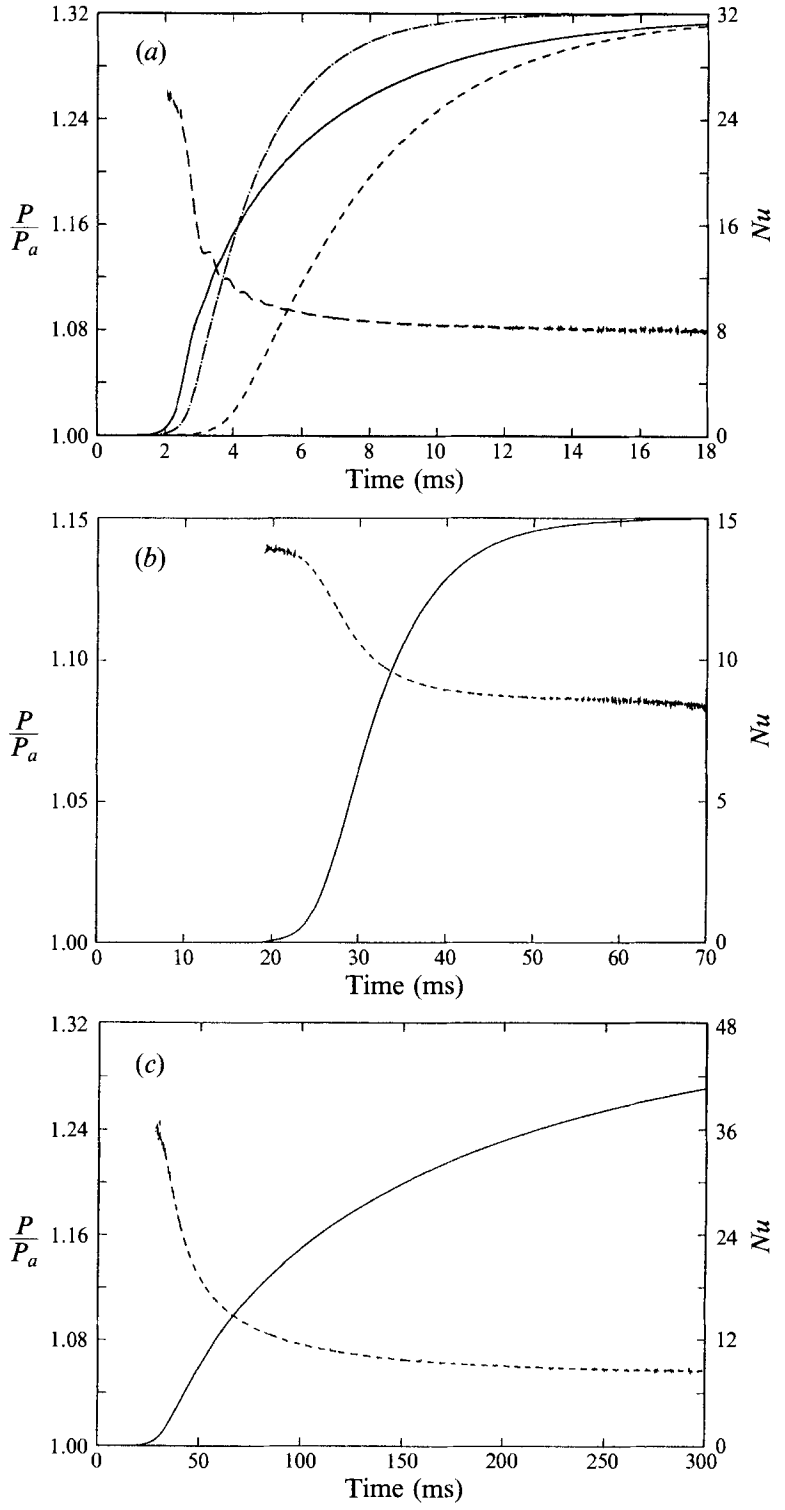

FIGURE 15. Waveform (solid line) and Nusselt number (dashed line) calculated according to (72) for the example of (*a*) figure 3, (*b*) figure 4(*a*), (*c*) figure 4(*b*). The solid line is the complete calculation, and in (*a*) the short-dashed line is the wave profile for $Nu = 10$, and the dash-and-dotted line the wave profile for $Nu = 20$.

where T_∞ is the undisturbed liquid temperature and $\langle T \rangle$ is the mass-weighted average gas temperature

$$\langle T \rangle = \frac{3}{R_a^3 \rho_a} \int_0^{R(t)} \rho T r^2 \, \mathrm{d}r = T_\infty \frac{pR^3}{p_a R_a^3}. \tag{73}$$

The dashed lines in figure 15 show this quantity for the shock waves of figures 3 and 4. It is evident that the complexity of the gas–liquid heat transfer gives rise to a strong variability of Nu along the wave. Aidagulov, Khabeev & Shagapov (1977) tested the approximation $Nu \sim$ constant against a full calculation based essentially on the same equations as here and concluded in its favour. We test this statement for the case of figure 3 in figure 15(*a*). Here the solid line is the full calculation, the short-dashed line the wave profile for $Nu = 10$, and the dash-and-dotted line the wave profile for $Nu = 20$. While the general form of the wave is preserved by the approximation, the detailed structure is not. We have reached similar conclusions for the other examples shown before.

The lines of figure 15 exhibit oscillations near the front and the back of the wave. These are actually numerical artifacts due to the fact that $\langle T \rangle$ is very close to T_∞ in these regions so that the division by their difference in (72) is inaccurate. To further examine this point we have calculated analytically the value of Nu near the wave front and back in the linearized approximation of §4 finding, near the back,

$$Nu_b = \frac{2}{3\gamma} \frac{\gamma - \kappa_b}{1 - \kappa_b} \Omega^2. \tag{74}$$

For the three examples of figure 15 this relation gives 7.976, 8.625, and 7.976 respectively, which agree very closely with the numerical results. (For the similarity between the first and third values compares the comment on κ_b in §4.3). Near the wave front

$$Nu_a = \frac{2}{3\gamma} \frac{\gamma - \kappa_a}{\kappa_a - 1} \Omega^2, \tag{75}$$

which gives the values 28.14, 14.05, 39.42. The substantial agreement with the computed results is clear also in this case in spite of the aforementioned numerical difficulties.

Another group of Russian researchers has been active in this area (see e.g. Kutznetsov *et al.* 1978*a*, *b*; Gasenko, Nakoryakov & Shreyber 1979; Nakoryakov, Shreyber & Gasenko 1981). They made use of a polytropic pressure–volume relation and of an effective liquid viscosity augmented to incorporate in an artificial way the effects of pressure radiation and gas–liquid heat transfer. Our detailed study of this approach (Prosperetti *et al.* 1988) demonstrates its dangers in the neighbourhood of nonlinear resonances for the case of a single bubble. Its accuracy for the motion caused by the propagation of pressure waves in a bubbly liquid has not been explored. These authors derived several approximate nonlinear wave equations (e.g. Korteweg–de Vries–Burgers, Boussinesq, and others) to describe phenomena in different ranges. Although they report a general consistency between their models and data, it is difficult on the basis of the results that they show to assess the degree with which this consistency extends to the quantitative realm. As a matter of fact, on the basis of our study, we are doubtful that the simplified approach they take to describe the gas–liquid interaction would result in any great accuracy. A similar mathematical model was used by Kedrinskii (1972, 1981) who studied the interesting problem of the interaction and transmission of a shock wave by a bubble layer, again finding a general consistency between theory and data.

Drumheller, Kipp & Bedford (1982) use a variational formulation to derive a set of averaged equations for bubbly liquids. They make a statement as to the importance of liquid compressibility which in their model appears in an *ad hoc* term. Although obtained from their variational scheme, this term is inconsistent with the correct formulation incorporated in (8) which is derived from first principles (Prosperetti & Lezzi 1986). To explore the importance of liquid compressibility we have compared simulations with finite and infinite values of the liquid speed of sound and found nearly indistinguishable results. It appears therefore likely that Drumheller *et al.*'s conclusion in this respect is vitiated by an incorrect incorporation of this effect in their mathematical model. Drumheller *et al.* also tried to model the thermal processes affecting the gas motion by appealing to linear theory, essentially (61) and (62). For this purpose they had to estimate a dominant frequency of the motion, and to interpret in a nonlinear context the complex result of the linear theory. This they did by taking the modulus, a procedure that evidently cannot take advantage of the important phase information contained in the linear result. Comparison with the data of Kutznetsov *et al.* (1978) has mixed success, while that with the data of Noordzij & van Wijngaarden (1974) is rather poor. In that study the theoretical gas pressure is compared with the measured liquid pressure. The difference between these quantities must be the entire left-hand side of the Keller (8) or Rayleigh–Plesset (30) equations and it is therefore unclear what to make of these results even for the cases in which agreement is claimed.

Tan & Bankoff (1984*a*) employed a standard two-fluid model in their study of very strong pressure waves in bubbly liquids. They essentially made use of a polytropic pressure–volume relation cast in the form of an effective energy equation. Their results exhibit the same behaviour as those of figure 2(*c*) and therefore, although no comparison with data was attempted in their paper, we feel justified in believing that a poor result would have been found had such a comparison been carried out. In another paper (Tan & Bankoff 1984*b*), these authors also present some experimental results on the speed of shock waves much stronger than those considered here. Since their tube was only 2.7 m long, their results must correspond to evolving waves although they were able to fit the measured shock velocities by the Campbell & Pitcher (1958) formula to within approximately 10%.

The most recent work on this subject is that of Beylich & Gülhan (1990), to whose data we have already referred. In their modelling these authors tried to incorporate a number of physical effects. Their mass and momentum equations are similar to (68) and (69), but the latter incorporates a 'turbulent' diffusivity for which, as already noted, they had to choose a value over 1000 times the molecular one in order to fit the amplitude of the oscillations. For the gas thermal behaviour, after some manipulations not unlike those used by Flynn (1975), they derived an approximate form inspired in its structure by the quasi-adiabatic approximation of Miksis & Ting (1984). Although their work goes beyond that of these authors, Beylich & Gülhan do not make use of systematic perturbation techniques and it is difficult to judge the accuracy of their final result. Our experience is that bubble behaviour depends critically on the gas energy equation and that even seemingly very reasonable approximations tend to introduce large errors (Prosperetti 1991; Kamath, Oğuz & Prosperetti 1992). Beylich & Gülhan also used a modification of the incompressible Rayleigh–Plesset equation with coefficients modified to take into account nearest-neighbour interactions. They found that their result for the wavelength of the oscillations was sensitive to the value chosen for these coefficients and, in order to match the data, they had to select not only a magnitude much bigger than that suggested by the study of Rubinstein (1985), but also with the opposite sign.

8. Conclusions

In our study of weak pressure waves in dilute bubbly liquids we have used a model containing all – and only – the effects important to first order in the bubble volume fraction. Our intent has been to explore the strengths and weaknesses of this limited, but mathematically well-justified, model, rather than to develop a more 'complete' one.

The comparison with experimental data measured sufficiently far from the initiation of the shock wave is in most cases very good. Where some disagreement exists, experimental error is a reasonable explanation. On the other hand, in the initial region, where the shock is thin and rapidly evolving, the theory does not compare well with data. An analysis of the most obvious effects – nonlinearities and relative motion between gas and liquid – shows that neither is sufficiently strong to account for the disagreement. Previous authors have also been faced by the same problem and had to have recourse to more or less *ad hoc* 'fixes' to match the data. It can thus fairly be stated that none of the models developed so far captures the physics of a thin and steeply rising pressure wave in a bubbly liquid. Beyond this negative result, we have unfortunately been unable to draw any conclusion as to nature of the physical processes whose omission prevents the models from matching the data. This evidently represents a major problem in the theory of bubbly liquids.

The thermal energy exchange between the bubbles and the liquid results in a rather unique dependence of the phase and group velocities upon frequency. It has been shown how this unusual dependence is responsible for much of the complexity and richness of the bubbly liquid behaviour.

The results presented here have been obtained for the somewhat artificial case of equal-size bubbles. The extension of the theory to a distribution of bubble radii is conceptually straightforward, although computationally demanding. As long as the timescale for the wave is much longer than the bubbles' resonance period, linear theory suggests that the effects of multiple bubble sizes should not be major. This however remains a potentially important point that must form the object of a separate investigation.

The authors are grateful to Professor L. Ostrovsky, Professor A. Beylich, and Professor Y. Matsumoto for several insightful conversations on the subject of this paper. This study has been supported by NSF under grant No. CTS-8918144 and DOE under grant No. DE-FG02-89ER14043.

REFERENCES

AIDAGULOV, R. R., KHABEEV, N. S. & SHAGAPOV, V. SH. 1977 Shock structure in a liquid containing gas bubbles with nonsteady interphase heat transfer. *J. Appl. Mech. Tech. Phys.* **18**, 334–340.

BEAM, R. M. & WARMING, R. F. 1976 An implicit finite-difference algorithm for hyperbolic systems in conservation-law form. *J. Comput. Phys.* **22**, 87–110.

BEYLICH, A. E. & GÜLHAN, A. 1990 On the structure of nonlinear waves in liquids with gas bubbles. *Phys. Fluids* A **2**, 1412–1428.

CAFLISCH, R. E., MIKSIS, M. J., PAPANICOLAOU, G. C. & TING, L. 1985 Effective equations for wave propagation in bubbly liquids. *J. Fluid Mech.* **153**, 259–273.

CAMPBELL, I. J. & PITCHER, A. S. 1958 Shock waves in a liquid containing gas bubbles. *Proc. R. Soc. Lond.* A **243**, 534–545.

COMMANDER, K. W. & PROSPERETTI, A. 1989 Linear pressure waves in bubbly liquids: Comparison between theory and experiments. *J. Acoust. Soc. Am.* **85**, 732–746.

DEVIN, C. 1959 Survey of thermal, radiation and viscous damping of pulsating air bubbles. *J. Acoust. Soc. Am.* **31**, 1654–1667.

DRUMHELLER, D. S., KIPP, M. E. & BEDFORD, A. 1982 Transient wave propagation in bubbly liquids. *J. Fluid Mech.* **119**, 347–365.

FLYNN, H. G. 1975 Cavitation dynamics I. A mathematical formulation. *J. Acoust. Soc. Am.* **57**, 1379–1396.

GASENKO, V. G., NAKORYAKOV, V. E. & SHREYBER, I. R. 1979 Nonlinear disturbances in a liquid containing gas bubbles. *Sov. Phys. Acoust.* **25**, 385–388.

JEFFREY, A. & KAWAHARA, T. 1982 *Asymptotic Methods in Nonlinear Wave Phenomena.* Pitman.

KAMATH, V., OĞUZ, H. N. & PROSPERETTI, A. 1992 Bubble oscillations in the nearly adiabatic limit. *J. Acoust. Soc. Am.* **92**, 2016–2023.

KAMATH, V. & PROSPERETTI, A. 1989 Numerical integration methods in gas-bubble dynamics. *J. Acoust. Soc. Am.* **85**, 1538–1548.

KAMATH, V., PROSPERETTI, A. & EGOLFOPOULOS, F. N. 1993 A theoretical study of sonoluminescence. *J. Acoust. Soc. Am.* **94**, 248–260.

KEDRINSKII, V. K. 1968 Propagation of perturbations in a liquid containing gas bubbles. *J. Appl. Mech. Tech. Phys.* **9**, 370–376.

KEDRINSKII, V. K. 1980 Shock waves in liquid containing gas bubbles. *Combust. Expl. Shock Waves* **16**, 495–504.

KELLER, J. B. & KOLODNER, I. I. 1956 Damping of underwater explosion bubble oscillations. *J. Appl. Phys.* **27**, 1152–1161.

KELLER, J. B. & MIKSIS, M. J. 1980 Bubble oscillations of large amplitude. *J. Acoust. Soc. Am.* **68**, 628–633.

KUTZNETSOV, V. V., NAKORYAKOV, V. E., POKUSAEV, B. G. & SHREIBER, I. R. 1978*a* Propagation of disturbances in a gas–liquid mixture. *Sov. Phys. Acoust.* **23**, 153–156.

KUTZNETSOV, V. V., NAKORYAKOV, V. E., POKUSAEV, B. G. & SHREIBER, I. R. 1978*b* Propagation of perturbations in a gas–liquid mixture. *J. Fluid Mech.* **85**, 85–96.

LIGHTHILL, J. 1978 *Waves in Fluids.* Cambridge University Press.

LU, N. Q. & PROSPERETTI, A. 1994 Active and passive acoustic behavior of bubbly layers. *J. Acoust. Soc. Am.* (in press).

MIKSIS, M. J. & TING, L. 1984 Nonlinear radial oscillations of a gas bubble including thermal effects. *J. Acoust. Soc. Am.* **76**, 897–906.

NAGIEV, F. B. & KHABEEV, N. S. 1979 Heat-transfer and phase–transition effects associated with oscillations of vapor-gas bubbles. *Sov. Phys. Acoust.* **25**, 148–152.

NAKORYAKOV, V. E., SHREYBER, I. R. & GASENKO, V. G. 1981 Moderate-strength waves in the liquids containing gas bubbles. *Fluid Mech. – Sov. Res.* **10**, 51–66.

NIGMATULIN, R. I. 1982 Mathematical modelling of bubbly liquid motion and hydrodynamical effects in wave propagation phenomena. *Appl. Sci. Res.* **38**, 267–289.

NIGMATULIN, R. I. 1991 *Dynamics of Multiphase Media.* Hemisphere.

NIGMATULIN, R. I. & KHABEEV, N. S. 1974 Heat exchange between a gas bubble and a liquid. *Fluid Dyn.* **9**, 759–764.

NIGMATULIN, R. I. & KHABEEV, N. S. 1977 Dynamics of vapor-gas bubbles. *Fluid Dyn.* **12**, 867–871.

NIGMATULIN, R. I., KHABEEV, N. S. & NGIEV, F. B. 1981 Dynamics, heat, and mass transfer in vapor–gas bubbles in a liquid. *Intl J. Heat Mass Transfer* **24**, 1033–1044.

NIGMATULIN, R. I. & SHAGAPOV, V. S. 1974 Structure of shock waves in a liquid containing gas bubbles. *Fluid Dyn.* **9**, 890–899.

NOORDZIJ, L. 1973 Shock waves in mixtures of liquids and air bubbles. Doctoral thesis, University of Twente.

NOORDZIJ, L. & WIJNGAARDEN, L. VAN 1974 Relaxation effects, caused by relative motion, on shock waves in gas-bubble/liquid mixtures. *J. Fluid Mech.* **66**, 115–143.

PLESSET, M. S. & PROSPERETTI, A. 1977 Bubble dynamics and cavitation. *Ann. Rev. Fluid Mech.* **9**, 145–185.

PROSPERETTI, A. 1984 Bubble phenomena in sound fields: part one. *Ultrasonics* **22**, 69–77.

PROSPERETTI, A. 1991 The thermal behaviour of oscillating gas bubbles. *J. Fluid Mech.* **222**, 587–616.

PROSPERETTI, A., CRUM, L. A. & COMMANDER, K. W. 1988 Nonlinear bubble dynamics. *J. Acoust. Soc. Am.* **83**, 502–514.

PROSPERETTI, A. & KIM, D. H. 1987 Pressure waves in bubbly liquids at small gas volume fractions. In *Fundamentals of Gas–Liquid Flows*, FED-Vol. 72 (ed. E. E. Michaelides & M. P. Sharma), pp. 19–27. ASME.

PROSPERETTI, A. & LEZZI, A. M. 1986 Bubble dynamics in a compressible liquid. Part 1. First-order theory. *J. Fluid Mech.* **168**, 457–478.

RUBINSTEIN, J. 1985 Bubble interaction effects on waves in bubbly liquids. *J. Acoust. Soc. Am.* **77**, 2061–2066.

SOD, G. A. 1978 A survey of several finite difference methods for systems of nonlinear hyperbolic conservation laws. *J. Comput. Phys.* **27**, 1–31.

TAN, M. J. & BANKOFF, S. G. 1984*a* Propagation of pressure waves in bubbly mixtures. *Phys. Fluids* **27**, 1362–1369.

TAN, M. J. & BANKOFF, S. G. 1984*b* Strong shock waves propagating through a bubbly mixture. *Exp. Fluids* **2**, 159–165.

WHITHAM, G. B. 1974 *Linear and Nonlinear Waves*. Wiley.

WIJNGAARDEN, L. VAN 1968 On the equations of motion for mixtures of liquid and gas bubbles. *J. Fluid Mech.* **33**, 465–474.

WIJNGAARDEN, L. VAN 1970 On the structure of shock waves in liquid-bubble mixtures. *Appl. Sci. Res.* **22**, 366–381.

WIJNGAARDEN, L. VAN 1972 One-dimensional flow of liquids containing small gas bubbles. *Ann. Rev. Fluid Mech.* **4**, 369–396.